Escola Tècnica Superior d'Enginyeries
Industrial i Aeronàutica de Terrassa
UNIVERSITAT POLITÈCNICA DE CATALUNYA

Degree: Aerospace Engineering

Course: 4th Grade Aerospacial Technologies Grade

Design and Performance Analysis Study of a Hall Effect Thruster

Contents: Report

Institution: Universitat Politècnica de Catalunya

Delivery Date: 13/06/2016

Student: MONILL GONZÁLEZ, Ricard

Director: LIZANDRA DALMASES, J. Oriol

Escola Tècnica Superior d'Enginyeries
Industrial i Aeronàutica de Terrassa

UNIVERSITAT POLITÈCNICA DE CATALUNYA

Design and Performance Analysis Study of a Hall Effect Thruster

Escola Tècnica Superior d'Enginyeria

Aeronàutica I Industrial

de Terrassa

Aerospacial Technologies Grade

Student: MONILL GONZÁLEZ, Ricard

Director: LIZANDRA DALMASES, J. Oriol

June 2016

Abstract

This study has two major purposes: one is to evaluate, using mathematical methods, whether the application of Hall Thrusters to transfer from LEO orbits to GEO is advantageous from economical and practical points of view or not, and the other is to introduce in the physics of magnetic plasmas and determine the physic processes and variations in parameters along the channel of a Hall Thruster developing a one-dimensional numerical method.

Data for this study were obtained from articles from different conferences about the field and documents and websites from space dedicated institutions such as NASA or ESA. Matlab code was constructed with the help and guidance of Prof. Lizandra, who provided facilities to document and understand Hall Thruster's physics.

Regarding the evaluation of LEO to GEO transfers, results show that Hall Thrusters are thoroughly advantageous in the economical field. Its high specific impulse permits reducing the amount of fuel needed in comparison with a conventional thruster, so having to launch less weight translates into a huge saving in money. However, in comparison to the few hours that a Hohmann transfer lasts, the month and a half that a low-thrust transfer can last seems like something to consider. In addition, the great number of times that a satellite orbits around the Earth when performing a low-thrust transfer exposes it to collisions and other problems.

On the other hand, on the basis of the result of the one-dimensional numerical model, it can be concluded that the variation of the key parameters along the channel of a Hall thruster is precisely predicted. In addition, the values of the parameters at the exit of the channel are the ones predicted by other theories. And the evolution with variable initial conditions were consistent and fitted the physic basic rules. Several modifications of the code for including a treatment for the plume, walls loses and two-dimensional effects are left for future works.

Analytical analysis showed that, despite the thrust grows when increasing the applied voltage, the efficiency reaches a maximum and falls. The point of maximum efficiency must be sought for greater performance.

Preface

Most communication satellites are placed in geostationary orbit (GEO). Taking them from the surface of the Earth to the final orbit is an expensive staged process which last stage is usually a transfer from a parking low-Earth orbit (LEO) to the final GEO destination.

New technologies in space propulsion have risen lately permitting reducing the cost of the mentioned last stage. As budgets in space missions are a major issue, private companies and governmental institutions are gaining interest in cheap revolutionary technologies. The aim of the project is study a popular space propulsion alternative such as Hall Thrusters. Both the performance in a LEO to GEO transfer and study of the physics inside the channel of the thruster using analytical and a one-dimensional numerical analysis are made.

Electric propulsion was first introduced at the first half of the XX century and highly developed during the Cold War both in USA and Soviet Union. In the last 10 years a rapid grow in the use of Hall thrusters in communications satellite and deep-space missions occurred. However, in the academic field, the efforts of study have been directed towards the understanding of ionization, electron trapping and diffusion, and loss mechanisms.

Developing this project has been a great challenge for me; diving in a filed totally unknown forced me to put a lot of effort in understanding the physics behind plasmas before being able to deal with the Hall Thruster itself.

I want to show special gratitude to my tutor Prof. Lizandra for his attention, help and guidance through the entire project, to the specialists Juan de Dalmau and Eduard Bosc from ESA and my uncle Ramón for introducing me to the electric propulsion field when I was lost.

It is impossible not to be grateful for the support of my parents Toni and Montse, my sister Anna, my family, friends and, specially, thanks to my girlfriend Clara for her contagious good energy and for showing me the bright side of life when all I could see was trouble.

Contents

List of figures

List of tables

Nomenclature

Orbit study

LEO	= Low Earth Orbit
GEO	= Geostationary Orbit
km	= kilometer
h	= hour
min	= minute
s	= Second
R_{Earth}	= radius of the Earth
r_{GEO}	= orbital radius of the geostationary orbit
h_{GEO}	= altitude of the geostationary orbit
P_{GEO}	= orbital period of the geostationary orbit
v_{GEO}	= linear velocity of an object orbiting in the geostationary orbit
μ	= Standard gravitational parameter
x	= spacecraft position in the axis of abscissas in an Earth-centered coordinate system
y	= spacecraft position in the ordinate axis in an Earth-centered coordinate system
v_x	= projection in the axis of abscissas of the velocity of the spacecraft in an Earth-centered coordinate system
v_y	= projection in the ordinate axis of the velocity of the spacecraft in an Earth-centered coordinate system
F_{T_x}	= projection in the axis of abscissas of the thrust of the spacecraft in an Earth-centered coordinate system
F_{T_y}	= projection in the ordinate axis of the thrust of the spacecraft in an Earth-centered coordinate system
a_T	= acceleration produced by the thrust
α	= angle between the radio vector and the ordinate axis in an Earth-centered coordinate system
r_{c_i}	= orbital radius of the initial circular orbit
r_{c_f}	= orbital radius of the final circular orbit

r_π = orbital radius in the perigee of the Hohmann transfer orbit

r_α = orbital radius in the apogee of the Hohmann transfer orbit

v_{c_i} = orbital velocity in the initial circular orbit

v_{c_f} = orbital velocity in the final circular orbit

a_H = semi-major axis of the Hohmann transfer elliptical orbit

v_π = orbital velocity in the perigee of the Hohmann transfer orbit

v_α = orbital velocity in the apogee of the Hohmann transfer orbit

t_H = flight time in the Hohmann transfer orbit

t_b = flight time in the low-thrust transfer orbit

m_{sc} = mass of the spacecraft

Isp = specific impulse

g_o = value of gravity at Earth's surface

m_i = initial mass of the spacecraft

m_f = final mass of the spacecraft

m_p = mass of propellant

$\dot{m}$ = mass flow of propellant

T = thrust of the Hall thruster

Hall thruster study

e = charge of an electron

E = value of the electrical field

m_i = Xenon's ion mass

v_i = velocity of the ions

m_e = electron's mass

v_e = velocity of the electrons

m_n = mass of a Xenon's neutral

v_n = velocity of the neutrals

$V(x)$ = electrical potential value depending on position

v_θ = electron orbital velocity

$\vec{B}$ = magnetic field

R_c = cyclotronic radius

ω_c = cyclotronic frequency

$\overrightarrow{J\theta}$ = Hall electric current

n_e = density of electrons

$\vec{f}$ = force produced by the Hall current

η = overall efficiency of the Hall thruster

I_a = array current

V_a = array voltage

F = Hall thruster's impulsive force

I_B = backstreaming current

A = radial section surface

n_i = ions density

n_n = neutrals density

υ_{en} = electron-neutral collision frequency

$\overline{c_e}$ = electrons' mean heat velocity

σ_o = characteristic surface

Γ_e = electrons flow

Γ_i = ions flow

Γ_n = neutrals flow

υ_{ion} = ion creation frequency

T_e = electron temperature

E_i = ionization energy

σ_{en} = electron-neutral collision characteristic surface

P_e = electron pressure

α_B = Bohm parameter

E_k = kinetic energy

E_i' = real ionization energy

X^* = any characteristic parameter for nondimensionalization

$\tilde{X}$ =any nondimensional parameter

v_{is} = sonic velocity

x_{ps} = thickness of the presheath zone

L = channel length

I_b = current of the beam

V_b = beam voltage

I^+ = current of the single ionized atoms

I^{++} = current of the double ionized atoms

α = correction parameter for double ionized atoms

β = correction parameter for beam divergence

γ = total correction parameter

1. Introduction

1.1. About Hall thrusters

Electric propulsion includes any technology in which electricity is used to increase the propellant exhaust velocity. Its main goal is to achieve thrust by using extremely high exhaust velocities with low mass flows, fact that reduces significantly the amount of propellant needed in a mission. The economic benefits of weight reduction are enormous as significantly smaller vehicles, which are also cheaper to launch, can perform the same missions as bigger vehicles with conventional propulsion.

The most used and the ones that have a brighter short term future among electrical propulsion systems are, without doubt, Hall thrusters. These thrusters can produce Specific Impulses from thousands of seconds to tens of thousands of seconds operating in power ranges of hundreds of watts up to tens of kilowatts, but generating thrusts of the order of some fraction of a single Newton. The propellant is any heavy inert gas, being Xenon the most popular.

The work mechanism of a Hall thruster is quite simple; they use a cross-field discharge described by the Hall effect to generate plasma, this is why they are called Hall thrusters. It is necessary an electric field in the direction of the motion of the particles that accelerates the ions to high exhaust velocities, and also a magnetic field, perpendicular to the previous one, that inhibits electron motion that would tend to short out the electric field.

Using this combination a higher thrust at a given power is obtained when comparing with other electric propulsion systems thanks to the simplicity and the fewer power supplies needed to operate.

According to what has been said, the objective of this project is to show that a Hall thruster can surpass a conventional one in terms of performance in certain missions. To do that a preliminary study of a Hall thruster will be developed.

1.2. State of the art

Electric propulsion itself was first mentioned at the US by Robert Goddard in 1906 (Goddart, 1906) and, independently in URSS by Tsiolkovsky in 1911 (Mel'kumov, 1911), but in none of the publications this electrical propulsion was related with space applications. It was some years later when Hermann Oberth in Germany in 1929 first, and then Shepherd and Cleaver in Britain in 1949 introduced several propulsion concepts with application in space missions.

The first appearance of Hall thrusters is not until the early 1960s again independently on the US (G. Seikel, 1962) and URSS (Yushmanov, 1958). But its investigation was abandoned in the US due to the discovery of some strong instabilities that could not possibly be eliminated coinciding with the appearance of works made by German scientists (Krulle & Zeyfang, 1975) indicated that the effective plasma collisionality that was theoretically predicted, was way lower than what really happened inside a thruster. In front of this situation, research efforts in West territories were focused to develop Kaufman type engines instead of Hall thrusters in missions with a determined specific impulse range.

Meanwhile, in the USSR, the bet on electric propulsion was strong and the development of Hall thrusters continued. The epicenter of all the work was the Kurchatov Institute in Moscow where, by designing more and more efficient configurations, realized that the instabilities, despite were real and very annoying, did not interfere with engine's performance. So in the 1960s and 1970s decades lots of experimental Hall thrusters were launched into orbit using first mercury or cesium propellants and developing progressively.

The first real application of electric was carried out by URSS scientist who launched a communication satellite incorporating Hall thrusters for orbit keeping (Boever, et al., 1991). Later, in 1971, the same soviet scientists launched a Meteor satellite equipped with two SPT-60s, which is one of the first Hall thrusters' models. Since those initial missions to date, almost 240 Hall thrusters have been operated in 48 Soviet/Russian spacecraft.

As Hall and ion thrusters' developments have always gone hand in hand, not only successful applications of Hall thrusters can be found but also ion thrusters. During the 1990s decade Japan their first satellites with ion thrusters for orbit keeping and gained experience for successfully provide the prime propulsion with an ion thruster for the Hayabuya asteroid mission sample maneuvers and return not many years ago. Also the United States regained interest in this kind of thrusters and launched in 1998 a probe called Deep Space 1 equipped with NSTAR, a self-designed ion thruster (Brophy, 2002).

The prosperity of ion thrusters has not stopped the developing and application of Hall thrusters worldwide. In Europe, for example, ESA used Snecma's PPS-1350-G Hall Thruster on SMART-1 mission to the moon (Koppel & Estublier, 2005). Meanwhile, Russian scientists have persisted on their idea of using Hall thrusters for orbit keeping purposes in communications satellites and plan to use these devices in future station keeping applications. The United States started later and it was not until 2004 when they first used a commercial Hall thruster, the Fakel SPT-100, in a spacecraft called MBSAT manufactured by Space Systems (Pidgeon, Corey, Sauer, & Day, 2006). However, they realized the future of these

technologies and have planned several launches in the next years equipped with commercial Hall thrusters.

To sum up, in the past 20 years a great growth in electric propulsion has been registered. Advanced Hall thrusters have emerged and proved to be an attractive and economic alternative to chemical thrusters in several missions. In the last 10 years a rapid grow in the use of Hall thrusters in communications satellite occurred. Both the United States and Russia have launched hundreds of the mentioned satellites equipped with Hall thrusters and will continue to do it in the future due to the possibility of reducing propellant mass for station keeping and orbit insertion. Another great application of electric propulsion that has grown a lot during the las ten years is deep-space missions. The possibility of obtaining high velocities with low propellant mass makes Hall thrusters very attractive for this kind of applications.

Finally, in the academic field, the efforts of study have been directed towards the understanding of ionization, electron trapping and diffusion, and loss mechanisms. To do that, it is necessary to explore the low power regime in order to miniaturize plasma propulsion for small probes. The principal difficulty is that, in small Hall thrusters, the violent plasma environment necessary to maintain a similar level of collisionality with larger devices reduces significantly the lifetime and efficiency of the thruster. Nowadays, however, it seems that the improvement on solar power systems is redirecting the investigation efforts towards high-power Hall thrusters.

1.3. Aim, structure and limitations

The main goal of this project is to develop a preliminary study of a Hall effect thruster for a spacecraft application.

As it is a preliminary study, and considering the lack of adequate infrastructures, not any physic test or real design will be made.

Due to time limitations, the study of the plume is not performed in any stage of the project, only the channel of the Hall thruster will be analyzed, and so the thrust and other parameters obtained must be corrected for plume and two-dimensional effects.

Matlab will be used for orbit trajectories and maneuvers computation, comparison with conventional propulsion systems, numerical analysis of a Hall thruster, results validations and some other computational tasks.

The project starts with an introduction to electric propulsion, the choice of a mission and different computations of the trajectory and spacecraft parameters using a Hall thruster and comparison with the same spacecraft with a

conventional thruster. Then a brief introduction to plasma physics is offered and followed by an analytic and numeric analysis of a Hall thruster which results are validated. Finally a numerical performance analysis is made and the conclusions extracted.

2. Mission Analysis

As it has been exposed, many applications for Hall thrusters have been developed in the recent years. Orbit keeping is the most popular, but also deep-space propulsion and approaching maneuvers are on the agenda.

Due to the incapability of producing high thrust, the situations where Hall thrusters can be used are quite limited. However, there is an extra application for these systems that most companies are working in because of the economic advantages it brings that is orbit transfer.

It is well known that telecommunication satellites are usually placed in GEO orbits. But satellites are not normally placed in the final orbit with a single maneuver. Most usually, there is a first transfer from the surface to a lower orbit, and a second transfer from the lower orbit to the final GEO destination. It is obviously impossible to perform both maneuvers with a Hall thruster, but the second interorbital transfer can be performed by one.

In this chapter, a trajectory study of the different ways to perform a transfer from a LEO to a GEO orbit with no inclination change is made.

2.1. Orbit description

2.1.1. Low Earth Orbits

LEO is and orbit situated in the region of space between Earth's surface and 2.000 km of altitude. As it is the only region where it is possible to send a manned mission and make it return in a reasonable time, it is also where the International Space Station or the Hubble Space Telescope conduct their operations, so that they can be visited by the Space Shuttle when needed.

Objects in LEO are over the atmosphere and below the inner Van Allen radiation belt, so they orbit inside the thermosphere if the orbit has between 80 and 500 km altitude or the exosphere if the altitude is over 500 km. Even though in the mentioned zones there is not enough air to breathe there are still some gases that cause the objects orbiting to receive a drag force. This drag slows down the objects making them lose energy and, as a result, there are pulled to the Earth.

In addition it is not a good region for satellites to orbit because the high speeds that the satellites need to turn around the Earth do not permit them to spend a reasonable long time over any part of the surface.

The best solution is to put the satellite in a Geostationary Orbit.

2.1.2. The Geostationary orbit

GEO is defined as a geosynchronous prograde orbit, what means that it is an orbit around the Earth with an orbital period matching the Earth's sidereal rotation period, in other words, the 23 h and 56 min that a sidereal day consists of and following the direction of the Earth's rotation. The inclination and eccentricity of this orbit are zero, meaning that any spacecraft orbiting in GEO is always directly above the Earth's equator and following a circular trajectory.

All the previous facts lead to that an object orbiting in a perfect GEO appears motionless in the sky. Even though a perfect GEO does not exist due to distortion forces caused by the Earth's asymmetry and not uniform mass distribution, it is a good approximation to consider it perfect because the magnitudes of this distortion are considerably low.

Knowing that the orbital period is a sidereal day and according to the second Kepler law

$$P_{GEO} = 2\pi \sqrt{\frac{{r_{GEO}}^3}{\mu}} \quad (1)$$

With the value of the Standard gravitational parameter

$$\mu = 3.986012 \cdot 10^5 \ km^3/s^2$$

The value of the radius and the altitude above the surface can be found

$$r_{GEO} = 42161.862 \ km$$

$$h_{GEO} = r_{GEO} - R_{Earth} = 35790.862 \ km$$

And with the radius, the linear velocity

$$v_{GEO} = \sqrt{\frac{\mu}{r_{GEO}}} = 3.075 \ km/s \quad (2)$$

A particular property that makes GEO very attractive for telecommunication satellites is the capacity to broadcast. The re-transmitted signal of the satellite can be picked up by antennas everywhere in the coverage area, and this coverage area for a satellite orbiting in GEO can be the size of a country, a continent or even a full hemisphere.

2.2. Transfer maneuver

There exist lots of different ways to transfer a spacecraft from a low parking orbit to a higher orbit using conventional propulsion. Depending on the strategy followed several parameters can be adapted. When talking about efficiency using a chemical thruster, the perfect transfer is Hohmann one.

On the other hand, regarding a transfer using a Hall thruster, there is no much option to choose due to the extremely low thrust that it provides.

In order to compute the trajectory followed by a spacecraft in a transfer orbit a four differential equation system needs to be solved. In Cartesian coordinates the system reads as follows.

$$\begin{cases} \dfrac{dx}{dt} = V_x \\ \dfrac{dy}{dt} = V_y \\ \dfrac{dV_x}{dt} = F_{T_x} + a_T \cdot cos\alpha \\ \dfrac{dV_y}{dt} = F_{T_y} + a_T \cdot sin\alpha \end{cases} \quad (3)$$

So what the code needs to do is solve this system for every step of time and, depending on the initial and in-flight conditions given, the trajectory will be one or another. The acceleration a_T is assumed constant despite the loss of fuel because the fuel lost is considerably smaller than the empty mass. However, to be able to solve that, some other considerations need to be done, geometrical relations for angle α and definitions of the value of F_T are indispensable.

$$\begin{cases} F_{T_x} = -\dfrac{\mu}{r^2} \cdot \dfrac{x}{r} \\ F_{T_y} = -\dfrac{\mu}{r^2} \cdot \dfrac{y}{r} \\ cos\alpha = \dfrac{V_x}{\sqrt{V_x^2 + V_y^2}} \\ sin\alpha = \dfrac{V_y}{\sqrt{V_x^2 + V_y^2}} \end{cases} \quad (4)$$

If the acceleration was not considered constant, since the thrust is actually constant, the expression for the acceleration would be

$$a_T = \frac{T}{m_o - \dot{m}t}$$

However, the change is so small that the figures would be nearly unaltered and the following study would leave to the same conclusions.

2.2.1. Conventional thruster: Hohmann transfer

A Hohmann transfer is an elliptical transfer between two co-planar circular orbits where only two impulses are made. The perigee of the mentioned elliptical transfer coincides with the inner orbit and the apogee with the outer orbit.

$$\begin{cases} r_{c_i} = r_\pi \\ r_{c_f} = r_\alpha \end{cases} \quad (5)$$

This fact makes this transfer orbit, which was discovered by a German scientist in 1925, the most fuel efficient way to make an interorbital transfer using chemical propulsion, a little lower thrust, and the spacecraft never reaches the final destination. Obviously, it is not the fastest way to change orbits, but when you are considering the use of electric propulsion the time should not be a main issue for the mission.

To have a perfect Hohmann transfer it needs to be assumed that there is no other gravitational attraction on the satellite than the Earth. Considering that neither another satellite sharing the orbit or a celestial body different from the one situated at the focus are disturbing the trajectory is a good assumption when transferring a satellite from a LEO to GEO, but needs further considering when talking about interplanetary transfers.

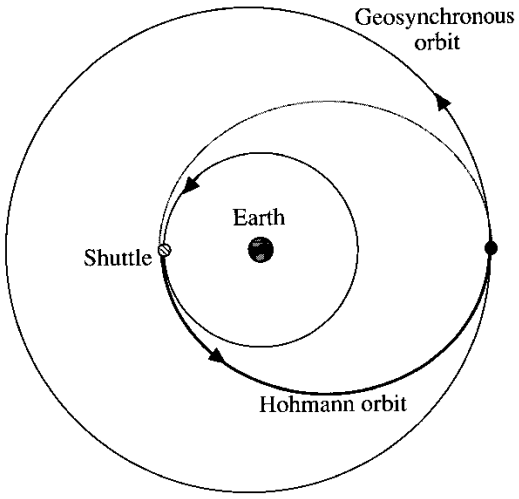

Figure 1. **Not scaled LEO to GEO Hohmann transfer (Case Western Reserve University, 2013)**

When considering a perfect Hohmann transfer, some equations can be written.

Considering the equilibrium between mechanical energy and the sum of potential and kinetic energies

$$-\frac{\mu}{2a} = -\frac{\mu}{a} + \frac{v^2}{2} \quad (6)$$

For the two circular orbits the semi-major axis a is equal to the orbital radius, so the orbital velocities can be isolated and read

$$v_{c_i} = \sqrt{\frac{\mu}{r_{c_i}}} \quad (7)$$

$$v_{c_f} = \sqrt{\frac{\mu}{r_{c_f}}} \quad (8)$$

Meanwhile, in the case of the ellipse, the semi-major axis is

$$a_H = \frac{r_\pi + r_\alpha}{2} \quad (9)$$

So, following the same methodology, the velocities at the perigee and apogee are

$$v_\pi^2 = \mu\left(\frac{2}{r_\pi} - \frac{2}{r_\pi + r_\alpha}\right) \quad (10)$$

$$v_\alpha^2 = \mu\left(\frac{2}{r_\alpha} - \frac{2}{r_\pi + r_\alpha}\right) \quad (11)$$

Now, once the previous and posterior velocities for both the punctual impulses made at the perigee and apogee are well known and remembering relation **(5)**, a mathematical expression for the needed change is detached

$$\Delta v_\pi = v_\pi - v_{c_i} = \sqrt{\frac{\mu}{r_{c_i}}}\left(\sqrt{\frac{2r_{c_f}}{r_{c_i} + r_{c_f}}} - 1\right) \quad (12)$$

$$\Delta v_\alpha = v_{cf} - v_\alpha = \sqrt{\frac{\mu}{r_{cf}}}\left(1 - \sqrt{\frac{2r_{c_i}}{r_{c_i} + r_{c_f}}}\right) \quad (13)$$

Some other interesting data of this transfer maneuver is the flying time. As a Hohmann transfer consists of exactly half an ellipse, the transfer time can be computed as exactly half the orbital period of the Hohmann ellipse using expression **(1)** applied to the orbit.

$$t_H = \frac{P_H}{2} = \pi\sqrt{\frac{\left(r_{c_i} + r_{c_f}\right)^3}{\mu}} \quad (14)$$

Using all the mentioned parameters, and with the construction of the Matlab code which refers to Hohmann transfers in Annex 1, the expected trajectory of a Hohmann transfer is proved.

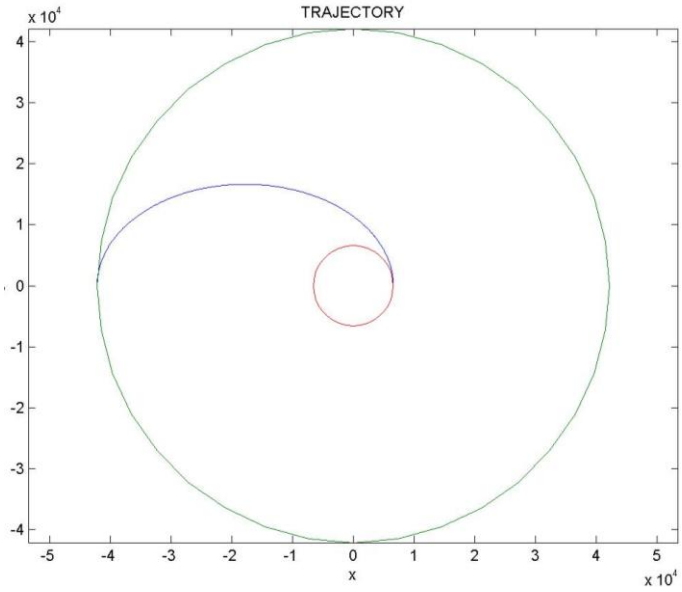

Figure 2. **Hohmann transfer from 200 km altitude LEO to GEO**

The figure above shows the trajectory followed in a Hohmann transfer from a 200 km altitude LEO to GEO. This one in particular has a transfer time of $1.8935 \cdot 10^4\ seconds$, in other words, $5\ hours\ 15\ minutes\ 35\ seconds$.

2.2.2. Hall thruster: low trust transfer

The orbit changes performed by Hall thrusters are way different from Hohmann transfers. The only reason is that, while chemical thrusters can give extremely high punctual thrusts, the thrust provided by a Hall thruster is typically under the tenth of a Newton, so it is not difficult to imagine how low accelerations are. All the previous facts make that the thrust time needs to be long, in fact the thrusters are fired for the entire duration of the maneuver.

For a significant orbit change, a low thrust transfer has a duration of the order of some months, so direct trajectories cannot be implemented, using low thrusts the unique way to achieve a transfer maneuver is with spiraling transfer trajectories. Meanwhile chemical propulsion directly inserts the spacecraft from the low to the higher orbit, a Hall thruster makes it orbit the Earth multiple times while slowly increasing its altitude.

In a maneuver with thrust provided during the full time of flight, as in this case, it is more difficult to quantify the change in velocity that the engine needs to provide. To simplify computation, it is accepted an approximation in which the acceleration provided by the thruster is constant on the entire maneuver, meaning that the weight loss is compensated by a variation of the value of the thrust. Thanks to this, the acceleration can be easily integrated along the whole travel time and the velocity variation provided obtained.

$$\Delta v = \int_0^{t_b} a_T \cdot dt \tag{15}$$

With the aim of understanding the type of transfer that is performed the equivalent code of the Hohmann transfer has been used, but adapted to the new in-flight conditions. In order to simplify the computation, it has been considered that the thrust given by the Hall thruster is always on the direction of the velocity of the spacecraft, what is a reasonable approximation. This code can be consulted in Annex 1 in the Low-Thrust Transfer section.

Just to see an example of the type of what this transfer looks like, as the study of the Hall thruster itself has not been made, it has been considered a medium typical value of thrust for a Hall thruster, not very optimistic but not pessimistic, of $300\ mN$. Also the medium weight of the aircraft has been estimated in$300\ kg$.

Using second Newton's law.

$$F_T = m_{sc} \cdot a_T \tag{16}$$

An estimated constant acceleration is obtained.

$$a_T = \frac{F_T}{m_{sc}} = \frac{0.3}{300} = 1 \cdot 10^{-3}\ m/s^2$$

Applying this acceleration over a period of time in the direction of motion the maneuver obtained is the following.

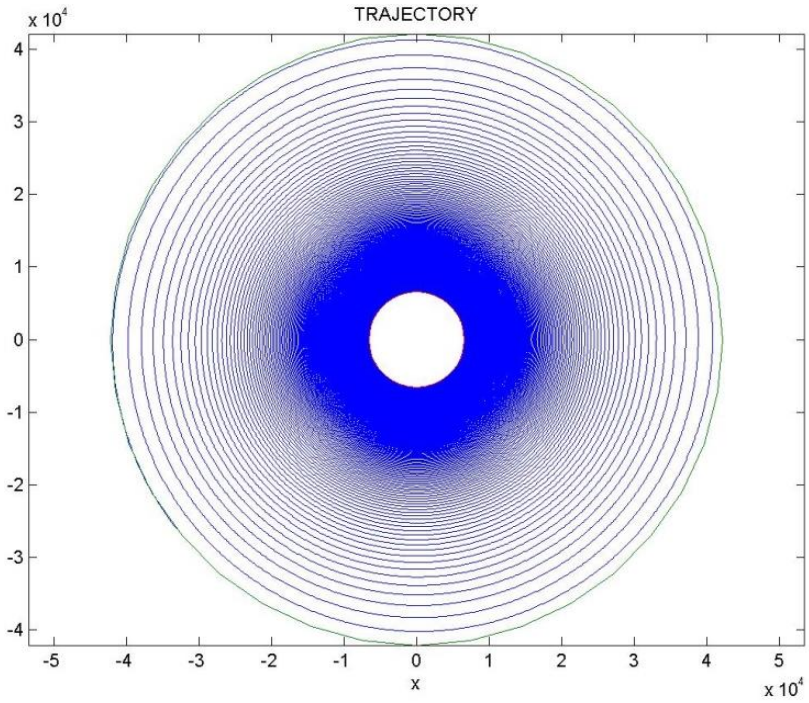

Figure 3. **Low-thrust climb maneuver from 200 km altitude LEO to GEO**

It can be observed a progressive and low climbing which gives the trajectory the spiral look and with a rate of climb that increases with the distance to the Earth.

The flight time of the maneuver in this case cannot be analytically found, but can be computed on Matlab thanks to the code developed. In this particular transfer with the same conditions as the previous one, from a 200 km altitude LEO to GEO, the transfer time is $4.7093 \cdot 10^6\ seconds$, in other words, $54\ days\ 12\ hours\ 8\ minutes\ 20\ seconds$.

Compared with the time of the Hohmann transfer it would seem that chemical propulsion is much better than Hall propulsion, but in the next chapter some relevant parameters will be analyzed and compared between the two transfers and some conclusions extracted.

3. Transfer Comparison

Once the different maneuvers and its physical principles have been exposed, a brief comparison is made in different fields. To do so, the same example as before has been chosen, a transfer from a 200 km altitude LEO orbit to GEO.

3.1. Evolution of parameters during maneuver

Some orbital parameters change during the course of the maneuver and the rate of change is different depending on the type of propulsion used and the characteristics of the thruster. In the present section the change of velocity and semi-major angles in different situations is evaluated.

3.1.1. Orbital velocity with time

In the case of the Hohmann transfer the evolution of velocity is the typical one in an elliptical orbit. In the specific case studied the distribution looks as follows.

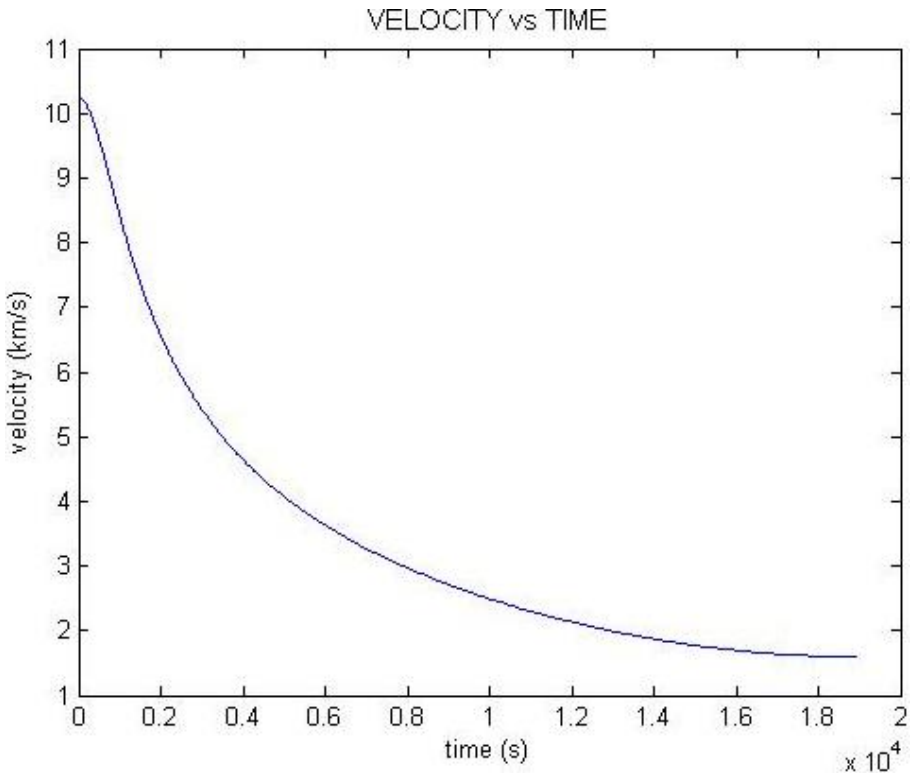

Figure 4. **Change of velocity in the Hohmann transfer orbit**

It can be observed that the rate of change in the velocity is higher at the initial stages when the spacecraft is closer to the Earth and the orbital velocities are higher.

It is important to notice that the velocities at the beginning and the end of the graph do not coincide with the orbital velocities in the initial and final circular orbits. This happens because it is precisely at the start and end of the process

where the two impulses are applied, and so, the goal of the mentioned impulses is to instantly change the velocity to leave the initial circular orbit and enter to the Hohmann transfer at the beginning, and to leave the Hohmann transfer and enter the final circular orbit at the end.

In the case of the low-thrust maneuver it is obvious that the change in velocity will depend on the acceleration that the thruster is giving but without affecting extreme values, as the final and initial orbits do not vary.

With the accepted approximation of constant acceleration in the direction of the motion it is not difficult to imagine that the graph velocity in front of time will be a straight line. To reduce computational effort a proposed expression can be assumed. (Stansbury, 2009)

$$v = \sqrt{v_{c_i}^2 - 2v_{c_i} \cdot a_T \cdot t + a_T^2 \cdot t^2} \qquad (17)$$

To understand the variation of the behavior of this expression under different thrust accelerations, three different reasonable accelerations have been applied, $a_T = 0.001\, m/s^2$, $a_T = 0.0005\, m/s^2$ and $a_T = 0.0001\, m/s^2$.

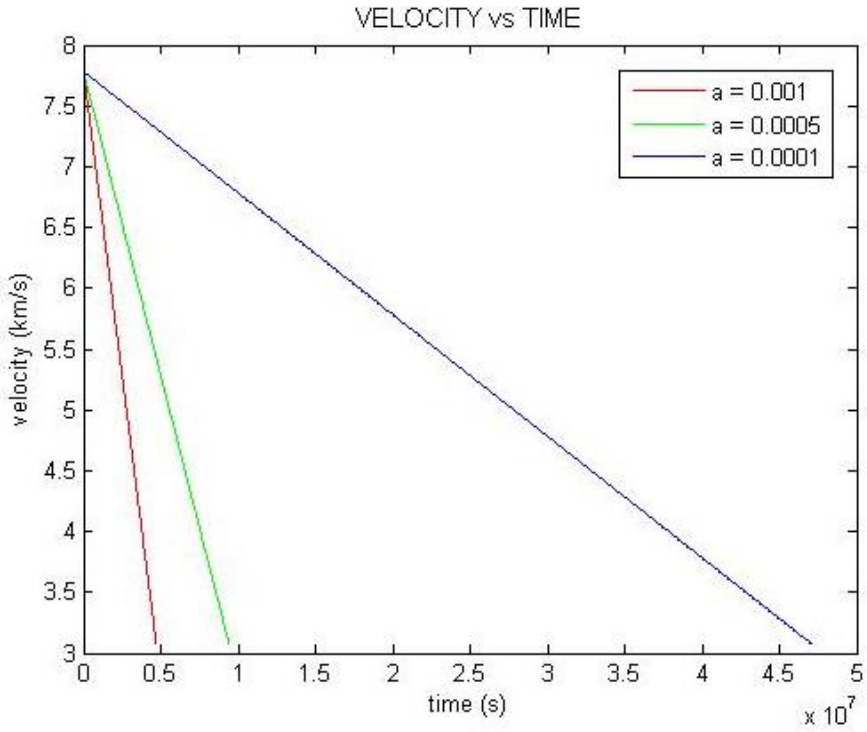

Figure 5. **Change of velocity in different cases of low-thrust transfer orbit**

As it can be noticed, the increase of the acceleration produces a drastic reduction of maneuvering time, because of this, on section 3.2, this effect will be further studied.

3.1.2. Semi-major axis with time

In the Hohmann case the semi-major axis is constant all along the maneuver because the spacecraft is always orbiting in the same elliptic orbit. But on the case of the low-thrust, as the thruster is acting during the whole maneuver, it can be considered that the spacecraft is in a different circular orbit every step of time.

In the figure below the Hohmann case is represented.

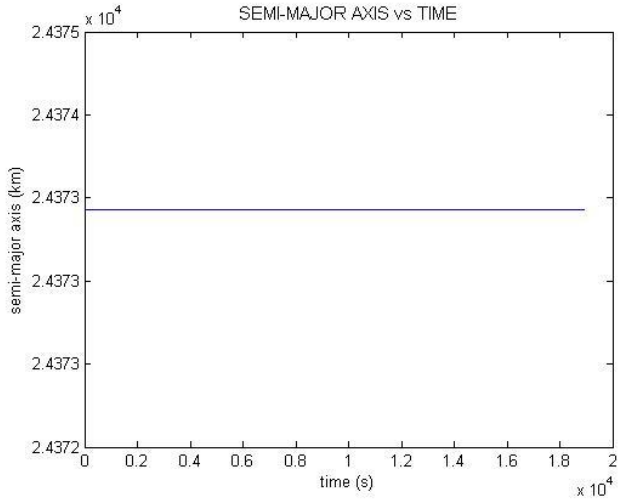

Figure 6. **Change of semi-major axis in the Hohmann transfer orbit**

Similarly to the velocity change with time, in the case of the low-thrust orbit, the change of semi-major axis strongly depends on the acceleration provided by the Hall thruster. So the same three different accelerations as before have been considered.

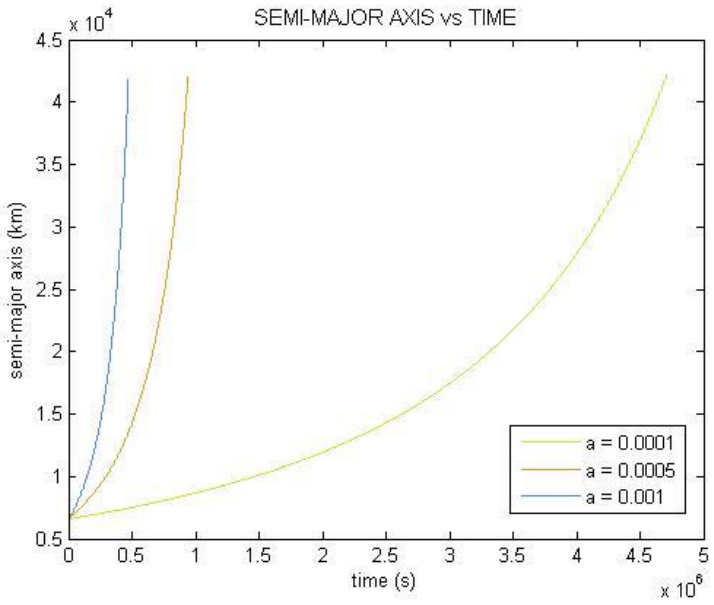

Figure 7. **Change of semi-major axis in different cases of low-thrust transfer orbit**

3.2. Maneuver time

One of the most important aspects in a transfer is the amount of time needed. Some missions have very strict timings of the different parts and it is essential to perform maneuvers as fast as possible.

Due to the importance of predicting the time that will be needed depending on the strategy followed, a brief analysis will be made in the following section.

3.2.1. Dependence on acceleration

In order to determine the behavior of maneuvering time for different accelerations the same situation as before is adopted; a transfer from a 200 km altitude LEO to GEO.

In first place it is important to notice that when talking about a Hohmann transfer dependence on acceleration makes no sense. This is because in a Hohmann transfer from 200 km altitude LEO to GEO the two punctual impulses are fixed and invariable, and the time needed to complete the maneuver is given by equation **(14)**.

As it was calculated before the time needed is

$$t_H = 1.8935 \cdot 10^4\ seconds = 5\ hours\ 15\ minutes\ 35\ seconds$$

On the other hand, it makes sense to talk of dependency on acceleration in low-thrust maneuvers. As it has been discovered above, the time needed to reach the final state of semi-major axis or velocity in a low-thrust maneuver descended considerably with the increase of acceleration. In fact, the complete dependence is showed on the figure below.

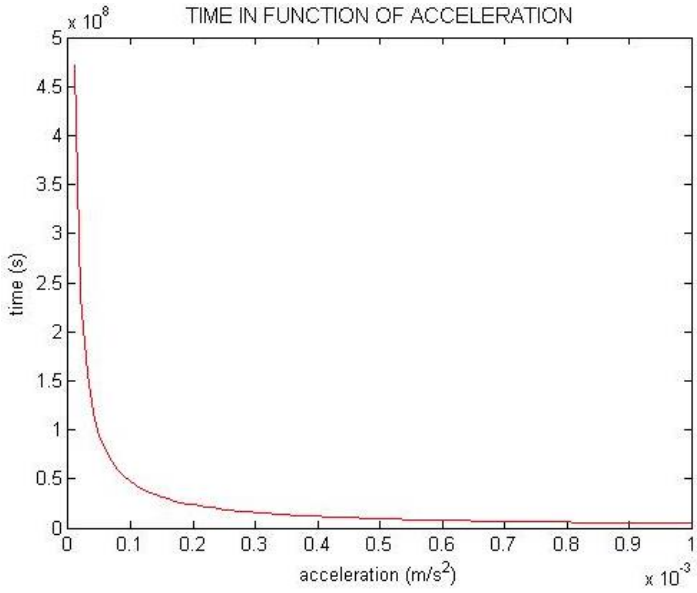

Figure 8. **Maneuver time in function of acceleration during flight**

The obvious result is obtained, when the acceleration becomes higher, the time needed to perform the transfer is reduced.

In the following table some numeric examples can be read.

Table 1. **Significant values of flying times for different accelerations**

Acceleration (m/s^2)	Time
0.0001	47,093,000 s (approx. 545 days)
0.0002	23,546,500 s (approx. 272.5 days)
0.0004	11,773,250 s (approx. 136 days)
0.0005	9,418,600 s (approx. 109 days)
0.0008	5,886,625 s (approx. 68 days)
0.001	4,709,300 s (approx. 54.5 days)

All the flight times for the considered accelerations are way higher than the Hohmann transfer one.

3.2.2. Dependence on initial altitude

For studying the effect of different initial altitudes, always in the range of LEO (0-2000 km), in the Hohmann transfer, no additional assumptions are needed, just the use of equation **(14)**. The graph obtained by applying the mentioned expression with different initial conditions is the following.

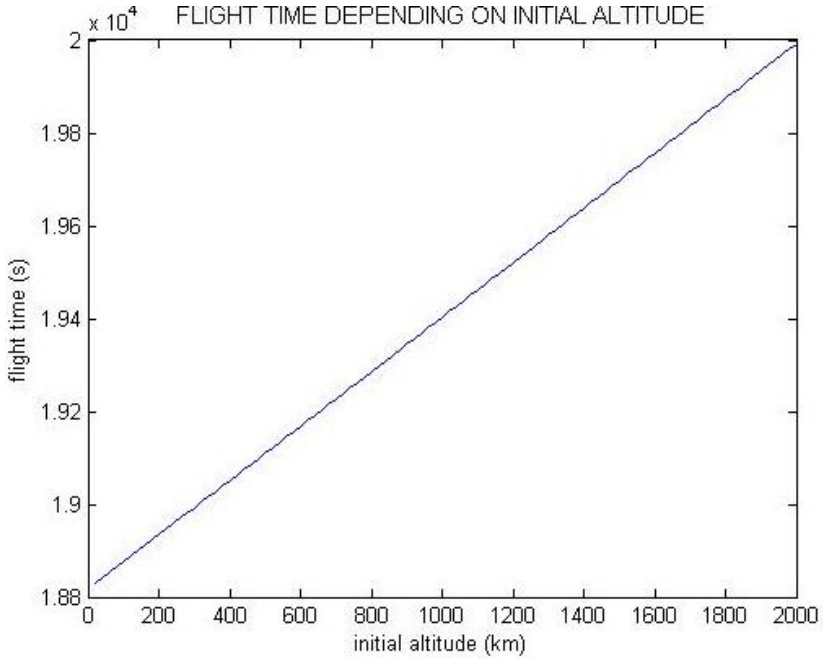

Figure 9. **Maneuver time in function initial altitude in Hohmann transfer**

Observing the result, a non-immediate behavior of the graph shows up. The higher is the initial orbit, meaning the closer it is to the final GEO orbit, the longer it takes to go from one to another. It is a surprising fact because an average human would say that if the orbits are closer, the time should be shorter. Let's see if low-thrust transfers follow the same pattern.

In order to obtain the equivalent graph of the figure above but with a low thrust transfer, the acceleration provided by the engines needs to be fixed. Again, the common value of $a_T = 0.001\ m/s^2$ has been used.

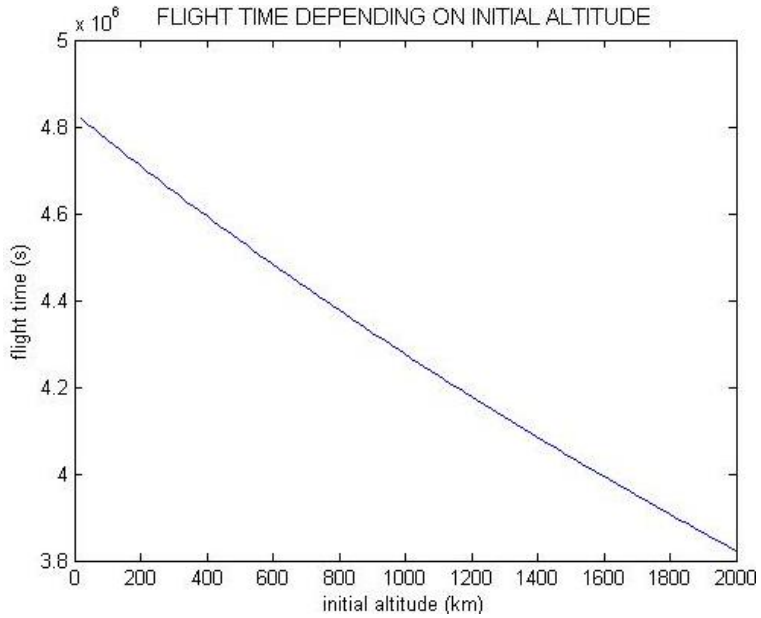

Figure 10. **Maneuver time in function initial altitude in low-thrust transfer**

The tendency observed in this case is clearly contrary to the one observed in Hohmann. With a low-thrust transfer, when the initial altitude is closer to the final altitude, the time of maneuvering reduces significantly. That happens because the thrust is applied continuously, so the spacecraft does not follow an orbit with a determinate mechanical energy, it is constantly changing its orbit and so, if the initial altitude is higher, the spacecraft has "less orbits" to change. Even though the graph seems as a straight line because of the short range of altitudes studied, it is not one. The gradient is higher at low altitudes because the closer the spacecraft is to the Earth, the stronger is gravity so it is more difficult for it to gain altitude and spends a longer time in those regions, as can be observed in **Figure 3.** Low-thrust climb maneuver from 200 km altitude LEO to GEO.

However, despite de different tendencies in both cases, the range of times with the Hohmann transfer is way lower than the one with the low-thrust maneuver. This fact is reflected in the table below that contains some examples of initial altitudes and compares both times.

Table 2. **Significant values of flying times for different altitudes and transfers.**

Initial altitude (km)	Transfer Time (Low Thrust)	Transfer Time (Hohmann)
200	4,593,631 s (approx. 53.17 days)	19,051 s (approx. 5.29 hours)
600	4,482,935 s (approx. 51.89 days)	19,168 s (approx. 5.32 hours)
1000	4,275,202 s (approx. 49.48 days)	19,403 s (approx. 5.39 hours)
1300	4,130,176 s (approx. 47.80 days)	19,579 s (approx. 5.44 hours)
1600	3,993,408 s (approx. 46.22 days)	19,756 s (approx. 5.49 hours)
1800	3,906,441 s (approx. 45.21 days)	19,874 s (approx. 5.52 hours)
2000	3,822,607 s (approx. 44.24 days)	19,993 s (approx. 5.55 hours)

It is important to see that in the Hohmann transfer, despite incrementing the transfer time with initial altitude, the difference of time between starting at an altitude of 200 km or 2000 km is just half an hour, a relative variation around 10% in respect of the flying time of nearly 5 hours.

On the other hand, the difference in the case of the low-thrust transfer is about 9 days, what supposes a nearly 20% of relative variation of the 53 initial days. Despite 20% of relative variation is not an enormous number, considering that the engines are working during all the way, 9 days can suppose a huge money saving.

3.3. Propellant consumption

If there is any parameter more important than time in a special mission it is the propellant consumption. Not only for the price of the propellant itself that is saved if the consumption is reduced, but because of the weight of its propellant. If the thruster needs more propellant to work, this propellant needs to be carried to space, and carrying extra weight to space is a synonym of a huge extra amount of money spent.

In order to have an approximated first idea of the propellant consumed in both maneuvers the ideal rocket expression presented by Tsiolkovsky is used, but with two different ways of expressing it.

When talking about Hohmann transfers the expression used is

$$\Delta v = Isp \cdot g_o \cdot ln\left(\frac{m_i}{m_f}\right) \quad (18)$$

Using the expression above is useful because the increments of velocity in a Hohmann transfer are easily found, so the only unknown is the mass ratio.

In the case of the low-thrust transfer it is more interesting to use the following way of writing the expression.

$$\dot{m} = \frac{T}{Isp \cdot g_o} \quad (19)$$

So that the mass flow can be easily computed by accepting that the thrust is constant all along the maneuver. This is not the same approximation that has been used in the previous sections, but it is also reasonable as, at it will be seen, the loss of mass on account of the propellant consumption is quite low.

Once the constant mass flow is known, it is easy to find the initial mass of the spacecraft.

$$m_i - m_f = t_b \cdot \dot{m} \quad (20)$$

The variation of this parameter in function of different facts is studied below.

3.3.1. Dependence on thrust

As it has been usual during the project, a transfer from a 200 km altitude LEO to GEO has been used to determine the dependence on thrust. Also the operational empty mass of the spacecraft has been estimated to be 300 kg.

However, it makes no sense to talk about dependence on thrust on a Hohmann transfer for the same reason as for the flight time. The fuel used is a fixed parameter in a determinate Hohmann transfer.

With aim of calculating the fuel used in our specific Hohmann transfer, the specific impulse of the chemical thruster has to be used so the value adopted is

$$Isp_c = 450\ s$$

It is the typical value for specific impulse in a chemical thruster that uses a mix between liquid oxygen and liquid hydrogen.

Also it is needed to know the total increment of velocity which follows the formula below.

$$\Delta v = |\Delta v_\alpha| + |\Delta v_\pi| \quad (21)$$

Where the increments of velocity at perigee and apogee can be extracted from equations **(12)** and **(13)**.

Using equation **(18)** and the considerations mentioned the initial and propellant masses can be calculated.

$$m_i = 731.05\ kg \rightarrow m_p = 431.05\ kg$$

In the case of the low-thrust transfer the specific impulse is way higher.

$$Isp_H = 2000\ s$$

It is an adequate specific impulse for a commercial Hall thruster nowadays. It is not very optimistic, but also not pessimistic.

With this information and computing equations **(19)** and **(20)** the following graph is obtained.

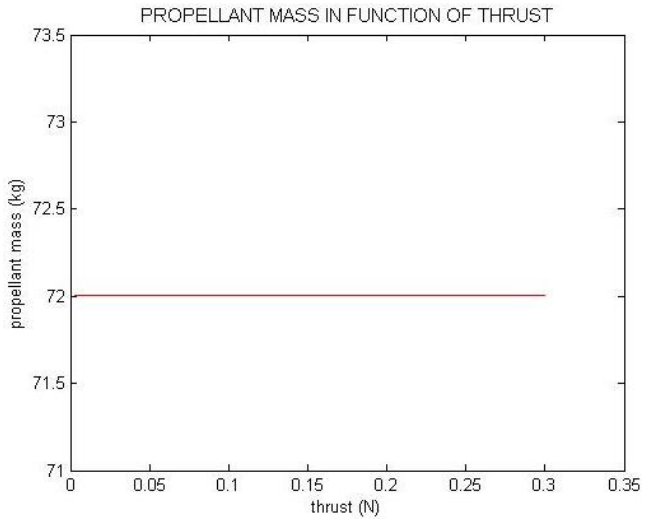

Figure 11. **Propellant used depending on thrust**

The result shows that independently of the thrust given, the propellant mass used is always the same. This is possible because when the thrust is higher, even though the propellant consumption increases, the time of flight diminishes, so the balance stays the same.

The value of the masses in the specific mission considered is

$$m_i = 372.01\ kg \rightarrow m_p = 72.01\ kg$$

What can be deduced is that, for a transfer mission, it will always be better the Hall thruster that provides the higher thrust, because, at equal specific impulses, the propellant consume will be the same.

3.3.2. Dependence on initial altitude

For studying the effect of different initial altitudes, always in the range of LEO (0-2000 km), in the Hohmann transfer, no additional assumptions are needed except for the specific impulse of 450 seconds and the use of equation **(18)**.

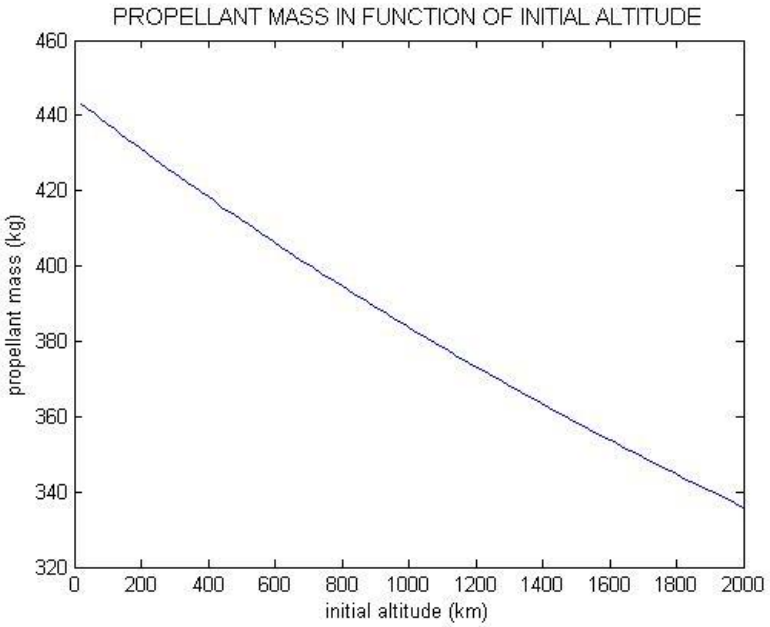

Figure 12. . **Propellant used in function of initial altitude in Hohmann transfer**

The behavior is the expected with less consume at higher initial altitudes.

If the low-thrust transfer is studied with the use of equations **(19)** and **(20)** it is necessary to fix a value of thrust. The value chosen for this study was:

$$T = 300\ mN = 0.3\ N$$

And the figure obtained with the specific impulse of 2000 seconds.

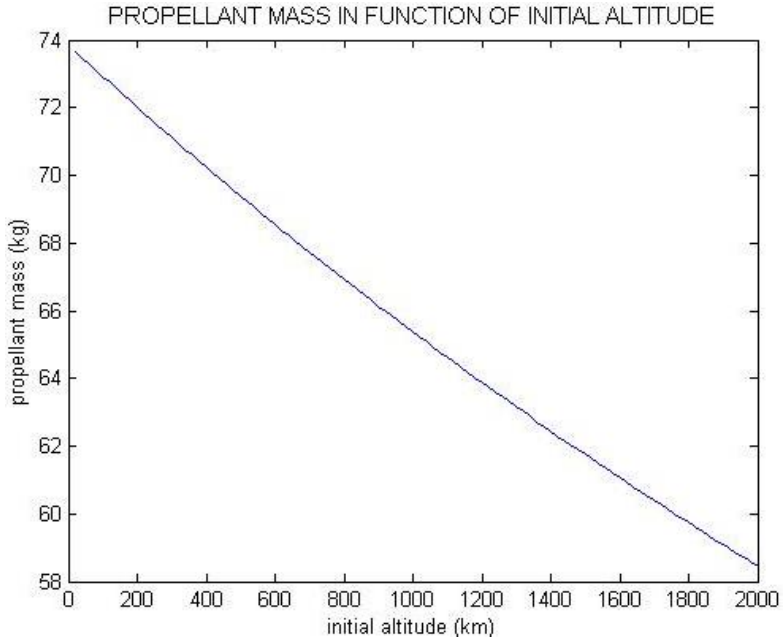

Figure 13. **Propellant used in function of initial altitude in low-thrust transfer**

The tendency observed is the same as in the Hohmann transfer so there is not much more to say about the figures. Let's see some values of propellant used and compare them.

Table 3. **Significant values of propellant consumed for different altitudes and transfers.**

Initial altitude (km)	Propellant Low Thrust (kg)	Propellant Hohmann (kg)
200	72.01	431.05
600	68.55	406.13
1000	65.37	383.65
1300	63.15	368.17
1600	61.01	353.73
1800	59.73	344.62
2000	58.45	335.90

According to the table, the consumption of propellant of a Hall thruster is much lower than a conventional one no matter the initial altitude. However, this difference becomes bigger at low altitudes, in other words, the longer the transfer is the more propellant is saved by using a Hall thruster in a spiral transfer.

3.4. Summary

The function of this section is to sum up all what has been studied on the previous chapters and finally compare the Hohmann orbit with the low-thrust transfer at all levels.

To do so, a constant acceleration of $a_T = 0.001\, m/s^2$ that the Hall thruster provides has been considered.

It is important to notice that the additional cost of carrying the extra fuel to the space is considered in the table. It is estimated that, nowadays, the cost of sending 1 kg of payload to the space is $30.000. (Stansbury, 2009)

If two examples of transfers from a 200 km and a 1600 km altitude LEO to GEO are used the results are the following.

For the 200 km initial altitude case.

Table 4. **Comparison of transfers with a 200 km altitude initial orbit to GEO**

Transfer type	Δv (km/s)	Maneuver time	Isp (s)	Empty mass (kg)	Propellant mass (kg)	Additional cost
Hohmann	3.93	5.25 hours	450	300	431.05	$ 10,771,200
Low-thrust	4.71	54.5 days	2000	300	72.01	---

And for the 1600 km initial altitude case.

Table 5. **Comparison of transfers with a 1600 km altitude initial orbit to GEO**

Transfer type	Δv (km/s)	Maneuver time	Isp (s)	Empty mass (kg)	Propellant mass (kg)	Additional cost
Hohmann	3.44	5.49 hours	450	300	353.73	$ 8,781,600
Low-thrust	3.99	46.2 days	2000	300	61.01	---

In conclusion, performing a low-thrust transfer is very slow because of the small amount of kinetic energy provided by the Hall thruster and with a higher increment of velocity needed as the thrusters act during the entire spiral trajectory. But, despite the previous facts, thanks to the enormous Isp provided by a Hall thruster in comparison with a conventional one the amount of propellant needed is lower. This weight save translates into some millions dollars save in payload transportation. An enormous amount of money that, by the way, increases with the distance of the transfer.

As additional information, approximated costs for the complete mission are presented for the sake of completeness. It is important to remark that these data have not been obtained by the present study, but recollected from references in order to give the reader an idea of the total cost of a communication satellite mission.

A table with the breakdown of operation costs of launching and using a communication satellite in a GEO orbit is presented for both propulsion options: whit a conventional thruster and Hall thruster.

In the case of conventional propulsion.

Table 6. **Cost breakdown conventional thruster communication satellite mission**

MISSION TOTAL		**289.4M €**
Satellite manufacture		**131.6M €**
Total launch		**105.3M €**
Ground to LEO		61.4M €
LEO to GEO		43.9M €
Total insurance		**35.0M €**
Launch insurance		17.5M €
In-orbit insurance		17.5M €
Operation costs		**17.5M €**
0.875M € / year	20 years	17.5M €

On the other hand, with the Hall thruster.

Table 7. **Cost breakdown Hall thruster communication satellite mission**

MISSION TOTAL		**274.6M €**
Satellite manufacture		**131.6M €**
Total launch		**96.4M €**
Ground to LEO		61.4M €
LEO to GEO		35.0M €
Total insurance		**30.6M €**
Launch insurance		17.5M €
In-orbit insurance		13.1M €
Operation costs		**16M €**
0.8M € / year	20 years	16M €

4. Brief Introduction to Magnetic Plasma Physics

In the previous chapters, different parameters of applications of low thrust in orbits have been studied. From now on, the study will be centered on the physics inside a Hall thruster.

4.1. What is plasma

As it has been mentioned before, a Hall thruster is a type of thruster that uses plasma physics to obtain thrust. To understand the internal operation of a Hall thruster it is essential to have a clear idea of what plasma is first.

In nature, electromagnetic forces tend to create structures like atoms or molecules. These structures are generally stable because its binding energies are greater than the external thermal energy. However, in a hotter environment, the larger stable structures like molecules start to decompose and, if the temperature is high enough to reach atomic ionization energies, even the atoms decompose in electrons with a negative charge and protons with a positive charge.

This does not mean that electrons and protons are free. They have a strong interaction between them caused by their electromagnetic fields. Even though, the charges are not bound, what means that they can assemble in multiple ways and be capable of complex collective motions. This mentioned assembly is what we call plasma.

While in a molecule the complexity relies on structure, plasma needs to be expressed both temporally and spatially, and it is characterized by the excitation of a wide range of collective dynamical modes.

Most plasmas found in nature are gases because the thermal decomposition breaks interorbital bound before starting ionization. That is the reason why most people define plasma like a gas that is ionized enough to exhibit plasma behaviors. In my opinion, though, this definition is not accurate, as the only to conditions to classify a substance as plasma are the presence of freely moving charged particles and an elevate number of them.

Plasma is not only made by electrons and protons, there are particles called neutrals that, despite their lack of electrical charge, can affect the system depending on their relative number. Similarly to charged particles, neutrals interact with other particles by means of electromagnetic interactions. However, it is considered that two neutral atoms do not affect one another until they collide, because forces between neutrals are short range. On the other hand, a charged particle produces a long range electromagnetic field that affects particles at long distances. Because of that fact, a single particle influences the whole system, so

it can be extracted that collective effects are very important to distinguish between a charged gas and plasma.

Most physicists say that 95% of the Universe is made of plasma. A sentence that is impossible to disprove or verify. However, what we know for sure is that in earlier stages of the Universe, everything was plasma. Even nowadays, stars, nebulae or even interstellar space are filled with plasma. The famous solar wind from our Sun is also plasma, and even Earth is surrounded by plasma trapped in its magnetic field.

Plasma can be found also in intra-atmospheric nature in lightnings for example. The study of plasma has led to the introduction of them in the industrial world. Plasma can be found in fluorescents and in some industrial processes, especially in micro-circuit fabrication.

4.2. Physics inside a Hall thruster

To understand the combination of phenomena occurring inside a Hall thruster it is important to schematically describe all of them. In the figure below, a visual approximation to the combination of factors can be observed.

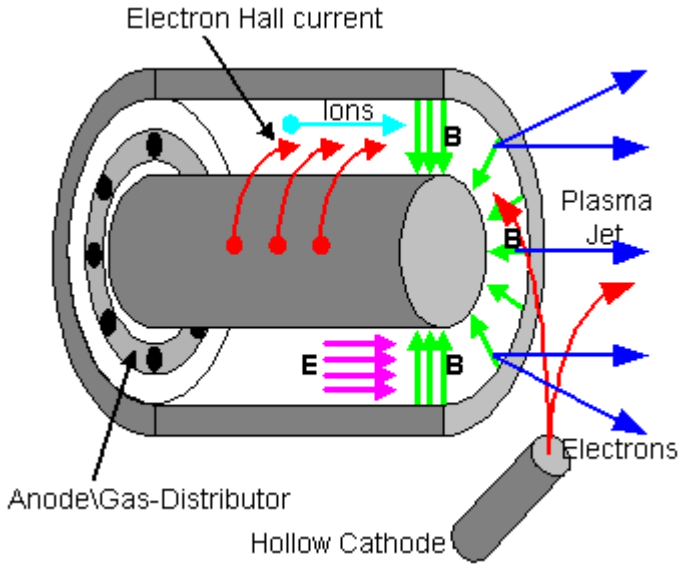

Figure 14. **Visual scheme of a Hall thruster (Jacob Blaustein Intitutes for Desert Research)**

Hall thruster is basically a coaxial annular cavity where plasma is created by passing electricity from the anode at the beginning to the cathode situated at the end, what creates an electric field in axial direction. The propellant is introduced into this cavity thanks to the gas distributor situated annularly in the same place as the anode. With only the existence of such electrical field, the electrons would travel directly from the cathode to the anode and the rate of collisions between electrons and propellant atoms would be very low, so the ionization process would be very inefficient. What is needed is a radial magnetic field, normally

using magnetic coils, that diminishes in great measure the axial velocity of electrons. The electrons are considered to be trapped by executing a $\vec{E} \times \vec{B}$ drift around the annulus.

On the other side, the ions are considered to be affected just by the electrostatic field. The low deviations caused by the magnetic field and collisions between ions can be neglected. Diving into the mathematical of the acceleration of the ions, the exit velocity expression can be found.

Starting by the equilibrium.

$$e\vec{E} \cdot d\vec{v} = d\left(\frac{1}{2}mv^2\right)$$

Introducing the potential of the electrical field in the equation.

$$e \cdot dV = d\left(\frac{1}{2}mv^2\right)$$

Integrating both sides.

$$e \cdot V + \frac{1}{2}mv^2 = cte.$$

Using the final conditions to obtain the value of the constant.

$$e \cdot V_x + \frac{1}{2}m{v_x}^2 = e \cdot V_{exit} + \frac{1}{2}m{v_i}^2$$

The desired velocity is v_i, the velocity of the ions at the exit. To find it, it is considered that, at the moment of ionization, the velocity of the atom is negligible and the potential of the electrical field at the exit is zero.

The expression obtained is as follows.

$$v_i = \sqrt{\frac{2eV(x)}{m_i}} \qquad (22)$$

Being $V(x)$ the potential at the place where the ion in question is created by the impact of an electron in comparison with the potential at the exit of the thruster. It is a parameter that varies depending on the electron considered. The earlier the proton is created, the longer space has to accelerate, and the greater exhaust velocity achieves, providing a higher thrust. The difficulty in knowing the value of $V(x)$ relies on determining the zones of major ionization of gas atoms. To do so, some functions are proposed as will be seen later.

Not all the electrons collide with an atom and ionize it. Some of them just slowly arrive to the anode due to the present electrical field and are pumped to the cathode by the power supply. These electrons are used to bombard the positive charged stream exiting the thruster and neutralize it. As it will be seen in the

following sections, not all those electrons neutralize the stream, some of them divert upstream into the cavity and produce losses.

It has been previously said that the ions are accelerated by the force of an electrical field. Somebody could think that the electrons present in the plasma to make it neutral would be accelerated with an opposite force towards the anode due to their negative charges. In fact, that would be true if it was not for the radial magnetic field. The presence of that magnetic field produces that the electrons are not free to accelerate towards the anode and drift azimuthally at a velocity that generates an equivalent centrifugal force to the magnetic force.

This velocity can be showed to be

$$\overrightarrow{v_\theta} = \frac{\vec{E} \times \vec{B}}{B^2} \qquad (23)$$

The direction of this velocity is easily understood in the figure below.

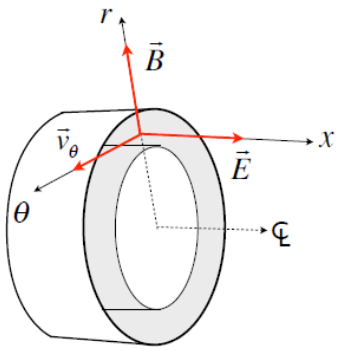

Figure 15. **Direction of fields and drift velocity (Martínez Sánchez)**

The radius of this circular motion can be easily found by applying the equality of centripetal and magnetic forces in absolute value.

$$e|\overrightarrow{v_\theta}| \cdot |\vec{B}| = m\frac{v_\theta^2}{R_c}$$

Where m can be the mass of both an electron and an ion and R_c is called the cyclotronic radius and has the expression

$$R_c = \frac{m}{e}\frac{v_\theta}{B} \qquad (24)$$

And defining the cyclotronic frequency

$$\omega_c = \frac{eB}{m} \qquad (25)$$

Expression **(24)** can be rewritten as

$$R_c = \frac{v_\theta}{\omega_c} \quad (26)$$

Someone can think that if the electrons follow this circular movement, the ions have to follow the opposite circular movement themselves as their polarity is the same as electrons with an opposite sign. In fact, they do have an azimuthal drift but, as an ion is thousands of times more massive than an electron, such will be its cyclotronic radius, being way larger than the thruster's length and so, producing no appreciable azimuthal drift.

The presence of this drift in electrons combined with the lack of drift in ions produces a net azimuthal current called Hall current, which gives name to the thruster itself. The expression of such current is:

$$\overrightarrow{J_\theta} = -en_e \frac{\vec{E} \times \vec{B}}{B^2} \quad (27)$$

The presence of a current inside a magnetic field generates a Lorentz force on the plasma that follows the expression

$$\vec{f} = \overrightarrow{J_\theta} \times \vec{B} \quad (28)$$

And rewriting expression **(28)** using equation **(27)**.

$$\vec{f} = en_e\vec{E} \quad (29)$$

Notice that the force received by the plasma follows the direction of the electrical field; hence the reaction force in the thruster follows the negative direction of the x axis.

5. Preliminary Analytic Analysis of a Hall thruster

As a previous step for the development of the numeric unidimensional model of a Hall thruster an analytic analysis is performed. This analysis will be basically based on the efficiencies of the thruster and the different variables involving the process of obtaining propulsion.

To do so, the simple and concise nomenclature proposed by Professor Martínez Sánchez will be used. (Martínez Sánchez)

The figure below gives a general outline of the nomenclature.

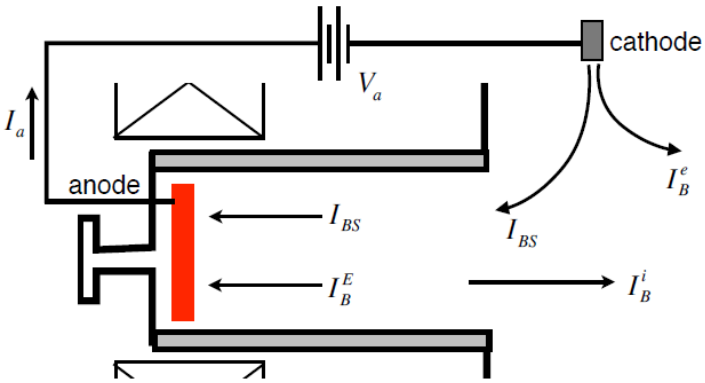

Figure 16. **Nomenclature proposed (Martínez Sánchez)**

5.1. Efficiency

An analytic analysis of a Hall thruster is basically based on the amount of power obtained in comparison with the amount of power given. The ratio between those two powers is called efficiency.

So an initial expression of the efficiency, following the notation presented above, could be

$$\eta = \frac{P_{obtained}}{P_{supply}} = \frac{\frac{1}{2}\dot{m}v^2}{I_a V_a} \quad (30)$$

Where P_{supply} is the external given electrical power and V_a and I_a are the voltage and intensity of current found in the power supply circuit respectively. It is important to notice that the electrons that form I_a current, once they arrive to the cathode, are divided into two different currents. Most of them have the mission of neutralizing the stream, and so, form a current I_B called beam current. However, some of the electrons deviate from the standard behavior and return to the anode forming what is known as the back-stream current I_{BS}, producing loss of efficiency as it will be seen later on. All in all, the intensities' relation reads

$$I_a = I_B + I_{BS} \quad (31)$$

For convenience in the further study expression **(30)** is rewrited in terms of the force obtained by the thruster.

$$\eta = \frac{F^2}{2\dot{m}V_a I_a} \tag{32}$$

The problem now relies on determining the value of this force. The thrust is only created by ions. The difficulty is that these ions are created in points of different potentials, and so are accelerated to different exit velocities given by the before mentioned expression **(22)**. So a general form to express this thrust is

$$F = \int v_i \cdot d\dot{m}_\iota \tag{33}$$

Note that as the thrust is only due to ions, it is only considered the ions' flow.

We confront a situation where two variables are found inside an integer. On the one hand there is the potential in the point of ionization $V(x)$ inside the term v_i and, on the other hand, the differential of ions flow $d\dot{m}_\iota$ itself. The only way to find a solution is using a relation between these two terms.

To obtain this relation an infinitesimal volume in the x direction is studied. It is considered that the part of ions flow $d\dot{m}_\iota$ is created in the zone where the electrical potential diminishes by dV. It is also mandatory to include a function f, called ionization distribution function, that adopts higher values at the areas of highest ionization and lower values in areas of low ionization. This function is not physically demonstrated and its value will be discussed later on.

So, taking into consideration all the pervious facts, the relation between variables is

$$\frac{d\dot{m}_\iota}{\dot{m}_\iota} = -f\left(\frac{V(x)}{V_a}\right)\frac{dV(x)}{V_a} \tag{34}$$

Following the advice of Professor Martínez Sánchez, a simple change of variable is applied to reduce complexity.

$$\phi = \frac{V(x)}{V_a}$$

And equation **(34)** is now

$$\frac{d\dot{m}_\iota}{\dot{m}_\iota} = -f(\phi)d\phi \tag{35}$$

Introducing equations **(22)** and **(35)** into the force expression **(33)**.

$$F = -\int_0^1 \dot{m}_\iota \sqrt{\frac{2eV(x)}{m_i}} f(\phi)d\phi$$

Multiplying the previous expression by the factor $\sqrt{\frac{V_a}{V_a}} = 1$, in order to simplify terms, a useful expression of the force is obtained.

$$F = -\dot{m}_\iota \sqrt{\frac{2eV_a}{m_i}} \int_0^1 \sqrt{\phi} f(\phi) d\phi \qquad (36)$$

At this point the new expression for the force **(36)** can be easily substituted into the efficiency equation **(32)**.

$$\eta = \frac{\left(-\dot{m}_\iota \sqrt{\frac{2eV_a}{m_i}} \int_0^1 \sqrt{\phi} f(\phi) d\phi\right)^2}{2\dot{m} V_a I_a}$$

Developing and simplifying what is obtained is

$$\eta = \frac{\dot{m}_\iota{}^2 e \left(\int_0^1 \sqrt{\phi} f(\phi) d\phi\right)^2}{m_i \dot{m} I_a} \qquad (37)$$

It is important not to forget the final purpose of this analytical approximation, which is none other than discussing the variation of efficiency in terms of different groups of related and characteristic parameters. So it would help to make appear another term with intensity of current in order to relate it to the current of the array.

Noticing that the group $\frac{e}{m_i}$ is found on the expression. One can relate the quotient charge of an ion (positive signed charge of an electron) divided its mass with the similar quotient total charge of the ions per unit of time divided its total mass per unit of time.

$$\frac{I_B}{\dot{m}_\iota} = \frac{e}{m_i}$$

Making I_B appear into expression **(37)**.

$$\eta = \frac{\dot{m}_\iota I_a \left(\int_0^1 \sqrt{\phi} f(\phi) d\phi\right)^2}{\dot{m} I_a}$$

And grouping

$$\eta = \left(\frac{\dot{m}_\iota}{\dot{m}}\right)\left(\frac{I_B}{I_a}\right)\left(\int_0^1 \sqrt{\phi} f(\phi) d\phi\right)^2 \qquad (38)$$

Three different factors are obtained. Their values vary depending on the configuration and accuracy of the Hall thruster considered, but the values adopted are always minor than 1. For this reason, these three factors are considered as independent efficiencies themselves.

5.1.1. Energy efficiency

The energy efficiency is a term produced by the lack of uniformity in the ionization of gas atoms. The energy efficiency is defined.

$$\eta_E = \left(\int_0^1 \sqrt{\phi} f(\phi) d\phi \right)^2 \quad (39)$$

It is important to remember what has been said in the previous section about the ionization distribution function $f(\phi)$. It adopts higher values at the areas of highest ionization and lower values in areas of low ionization, and it is incorporated in the expression without modifying the value of the differential itself, meaning that has an unitary value, so it is quite clear the condition

$$\int_0^1 f(\phi) d\phi = 1 \quad (40)$$

Taking into consideration expressions **(39)** and **(40)** one can extract that the energy efficiency term will be higher when the ionization distribution function $f(\phi)$ is mostly distributed in high potential (so high ϕ) regions.

Thinking about it physically, it seems obvious that if the ionization of the atoms mostly happens near the anode, the created ions have longer distances to accelerate and so, reach higher kinetic energies.

Following this criteria, the point of maximum energy efficiency should be reached when all the ionization happens exactly near the anode. This means that the ionization distribution function has to be completely contained in the same position as the anode, in other words, it has to be a Dirac function centered at the initial point.

$$f_{\eta_E^{max}}(\phi) = \delta(\phi - 1)$$

Function that leads to the obvious result of

$$\eta_E^{max} = \left(\sqrt{1} f(1) \right)^2 = 1 \quad (41)$$

Obviously, the lack of ionization would lead to an overall zero energy efficiency.

Another simple case that can be studied analytically, but clearly more accurate to reality than the previous one is considering the ionization constant along the chamber.

$$f_{hom}(\phi) = 1$$

According to equation **(35)**, this ionization distribution function produces that the decrease of electrical potential along the chamber is directly proportional to the increase in ions' mass flow. So, equation **(39)** in this particular case.

$$\eta_E^{hom} = \left(\int_0^1 \sqrt{\phi} d\phi\right)^2 = \left(\frac{2}{3}\right)^2 = \frac{4}{9} \cong 0.44 \quad (42)$$

However, this value continues to be different from reality. Experimental measures (Komurasaki, Hirakowa, & Arakawa, 1991) have proven to be the homogenous approximation as a pessimistic scenario. Real Hall thrusters have energy efficiency values normally between 0.6 and 0.9, what means that ionization tends to occur early in the chamber, a logical fact considering that in these regions the backstream electrons have gained more energy.

All in all, this value continues to be hard to estimate because it depends on the specific geometry of the Hall thruster considered or its array's working conditions. It can also suffer slight variations when studying a single Hall thruster due to the intervention of probability.

5.1.2. Utilization factor

The utilization factor is, indeed, the fraction of ionized flow. So it is defined as follows.

$$\eta_u = \frac{\dot{m}_\iota}{\dot{m}} \quad (43)$$

Breaking down the denominator, which is composed by the sum of ions and neutrals flow

$$\eta_u = \frac{\dot{m}_\iota}{\dot{m}} = \frac{\dot{m}_\iota}{\dot{m}_\iota + \dot{m}_n}$$

And knowing that every flow is defined by the product of density of particles, the mean velocity of the particles and the transversal area

$$\eta_u = \frac{n_i v_i A}{n_i v_i A + n_n v_n A} = \frac{n_i v_i}{n_i v_i + n_n v_n}$$

It is important to notice that the density of ions is equivalent to the density of electrons because an ion is created by detaching an electron from a neutral. So the appearance of an ion walks hand in hand with the appearance of an electron, which leaves to the mathematical equivalence $n_e = n_i$. Taking the previous fact into consideration and multiplying by the factor $\frac{1}{n_n v_n}$ the numerator and denominator

$$\eta_u = \frac{\left(\frac{n_e}{n_n}\right)\left(\frac{v_i}{v_n}\right)}{\left(\frac{n_e}{n_n}\right)\left(\frac{v_i}{v_n}\right) + 1} \quad (44)$$

Since normally no more than 10% of the neutrals are ionized $(n_e/n_n \sim 0.1)$, it is fair to think, at first sight, that the utilization factor will never be high. However, when analyzing the velocities' quotient term, one can realize that the utilization factor can be high since ions reach velocities of tens of thousands meters per second while neutrals reach only a few hundreds of meters per seconds.

In fact, experimental data (Ahedo & Martínez-Sánchez) show that typical utilization factor oscillate between 0.4 and 0.9 depending on the model of Hall thruster.

5.1.3. Backstreaming or anode efficiency

It is, in my opinion, more accurate to call this factor anode efficiency because it is defined as the fraction of array current that is used to neutralize the beam.

$$\eta_a = \frac{I_B}{I_a} \tag{45}$$

A conflict of interests is found when trying to maximize this term. Most of the ionization is produced thanks to the back-streaming electrons that collide with ions. So making I_B tend to I_a would make the backstream current (I_{BS}) to zero, and so, there would be no ionization making the utilization factor **(43)** and, consequently, the total efficiency **(38)** be zero.

Taking into consideration this relation between the anode efficiency and the utilization factor and knowing that they cannot be maximized both at the same time, what has to be done is find an intermediate solution.

Paying the price of having some backstream electrons (anode efficiency less than 1) what increases the overall efficiency of the Hall thruster is taking the maximum profit of them. This fact relies on the creation of the maximum number of ions by action of the mentioned backstream electrons and preventing losses on the walls by recombination of created ions and single electrons.

To increase ionization it is recommendable to use accelerating potentials that have been proved experimentally as highly ionization efficient. However, for heavy atoms, these potentials cannot be used because are too low to accelerate to a given exit speed the ions. Another way is to lower the electrons' drift velocity, in other words, increase the electrons path by adjusting the radial magnetic field.

On the other hand, the surface of insulating materials used, which are zones where recombination takes place, must be minimized. And also have a great control over equipotential surfaces so that ions are not accelerated towards the wall.

5.2. Thrust limit

Until now, only the parameters that maximize efficiency have been studied. But what about the thrust that a Hall thruster provides? Considering the definition of efficiency in expression **(38)**, is it possible to increase the mass flow maintaining the ionization ratio and achieve a level of thrust as high as you want? The answer is no.

To find some restrictions to the thrust it is essential to study the collisionality frequency between electrons and heavy particles as neutrals. As it will be shown later on, it follows the expression below.

$$\nu_{en} = n_n \bar{c_e} \sigma_o \qquad (46)$$

Where n_n is the density of neutrals, $\bar{c_e}$ is the mean thermal velocity of electrons and σ_o is a collision surface which value depends on the gas used.

When this frequency becomes comparable to the cyclotronic frequency of electrons **(25)** electrons no longer maintain an azimuthal drift. The high density of collisions allows the electrical field to push the electrons towards the anode crossing the magnetic barrier.

Some studies (Dan Goebel, 2008) propose the following expression for the upstream velocity of the electrons in the mentioned conditions.

$$v_{e_x} = \frac{E}{B} \frac{\upsilon_{en}}{\omega_{ce}} \qquad (47)$$

This flow of electrons produces what is called a leaked current that has a value

$$I_{leak} = e n_e \frac{E}{B} \frac{\upsilon_{en}}{\omega_{ce}} \qquad (48)$$

In this case, the leaked current is equivalent to the back-streaming current that has been mentioned all along the previous part. So it is found that the back-streaming current increases directly with n_n due to the υ_{en} contribution. Increasing the mass flow automatically increases the density of neutrals n_n so, consequently, it can be affirmed that increasing the mass flow supposes also increase the leaked current.

If the anode efficiency expression **(45)** is remembered and developed.

$$\eta_a = \frac{I_B}{I_a} = \frac{I_a - I_{leak}}{I_a} = \frac{1}{1 + \frac{I_{leak}}{I_B}}$$

In conditions where υ_{en} and ω_{ce} have equivalent values, the effect of high collisionality between electrons and neutrals produces that, by increasing the mass flow, the leaked current increases faster than the current used to neutralize

the beam due to the proportionality of the leaked current to the density of neutrals.

So, according to the expression above, the efficiency of the thruster diminishes when increasing the mass flow. This fact is, without doubt, a strong limitation to the maximum thrust that a Hall thruster can achieve.

5.3. Verification with experimental results

The predicted tendencies can be verified with the use of results obtained by numeric and experimental analysis. (Garrigues, Boyd, & Boeuf, 2001)

The article mentioned presents a table with different efficiencies for different voltages of the array using Xenon.

Table 8. **Efficiencies for different array voltages. (Garrigues, Boyd, & Boeuf, 2001)**

V_a	η_u (%)	η_a (%)	η_E (%)	η (%)
150	44.1	95.6	50.5	21.3
200	72.5	96.5	46.0	32.2
250	85.5	95.5	46.1	37.6
300	89.7	96.3	47.6	41.0
350	94.4	95.6	43.0	38.8
400	96.6	95.3	40.0	36.8

If the table above is plotted

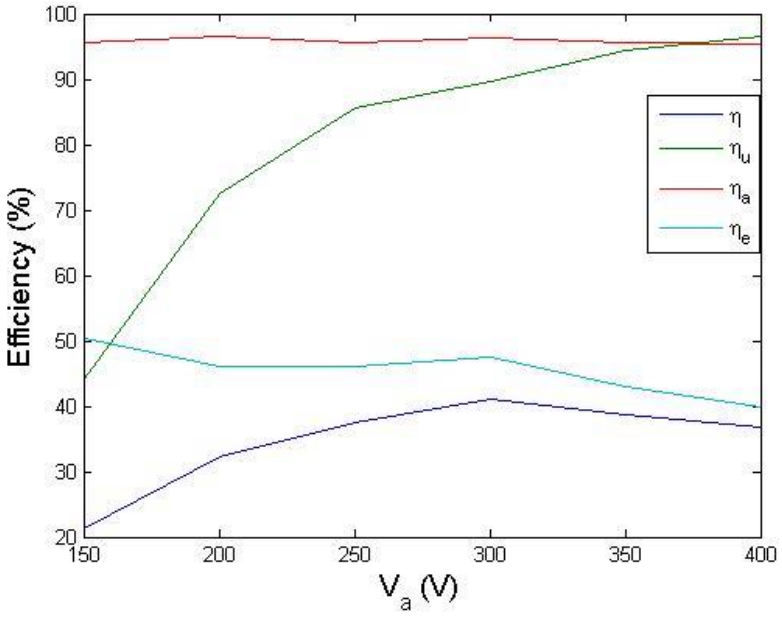

Figure 17. **Evolution of efficiencies with input voltage.**

The anode efficiency η_a maintains constant because, despite the variation of voltage on the array produces a variation on the intensity of the array, the fraction of this current used to neutralize the beam is the same. As expected, this efficiency has a high value (close to 1) because that means reducing the backstream current, the principal source of losses.

The utilization factor η_u increases with the voltage array. It is a reasonable behavior as the combination of electrical and magnetic field traps the electrons. If this electrical field is stronger the electrons will be closely trapped and collisions between neutrals and them will be more likely to increase, so ionization increases as expected. However, in **Figure 17.** Evolution of efficiencies with input voltage., it is observed that the growing rate of this factor diminishes with high voltages; it tends to stabilize to a high value but never reaching 1, because complete ionization is impossible.

The energy efficiency η_E slightly diminishes but is nearly constant. That means that, despite the change of input voltage, ionization happens mostly in the same zone.

Finally, the overall efficiency η grows at the beginning, but seems to reach a maximum and then descend as it was expected by the given analytic expressions. This maximum is reached when the ionization fraction is stabilized and the opposing effects become stronger.

The analytical analysis of the previous section also says that the maximum thrust of a Hall thruster is limited. It reaches a maximum but then the efficiency starts falling and so does the thrust provided despite the mass flow or the input voltage continue growing.

Some experimental analysis (Garrigues, Boyd, & Boeuf, 2001) show the following figure

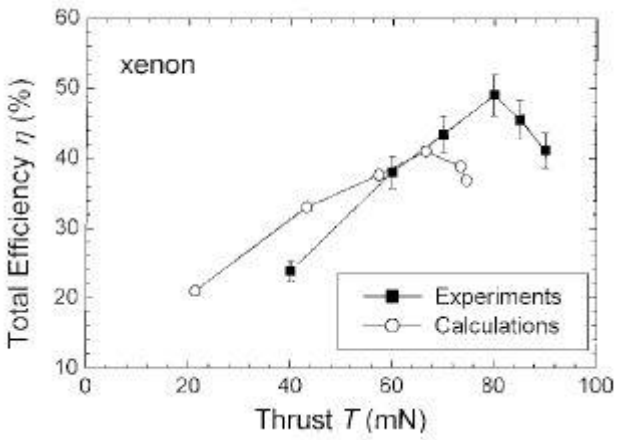

Figure 18. **Total efficiency variation with thrust. (Garrigues, Boyd, & Boeuf, 2001)**

Figure 18. Total efficiency variation with thrust shows that there is a value of thrust for which the efficiency reaches a maximum and, from that point on, the efficiency falls rapidly. For higher thrusts, the power needed in the array is much higher in percent to the power obtained that for optimized efficiency thrusts. This fact verifies the thrust limit expected, the thrust cannot grow forever because the efficiency drops to very low values.

Most Hall thrusters are prepared to work on optimal thrust to efficiency conditions, however, reasonable higher thrust can be obtained paying the price of having worse efficiency.

6. Numeric Analysis of a Hall thruster

Once understood the beneficial parameters for the performance of a Hall thruster it is time to develop a deeper study.

To do so, a one-dimensional numeric model of a Hall thruster proposed by Ahedo and Martínez-Sánchez in their article "One-dimensional Plasma Structure in Hall Thrusters" (Ahedo & Martínez-Sánchez) has been used.

This model is based on the treatment of electrons as a fluid, but treating the ions as particles. Further mathematical demonstration of why this approximation is reasonable is not provided in these sections, but can be found in articles (Ahedo & Martínez-Sánchez) and books (Dan Goebel, 2008) mentioned in the literature.

Treating the electrons as a fluid permits formulating mass, momentum and energy conservation equations. On the other hand, treating the ions as particles only permits formulating mass and momentum conservation equations. The energy equation in the case of ions is redundant of the momentum equation.

The mathematical fundaments and development needed to write a Matlab code are presented organized in the sections below.

6.1. Previous considerations

First of all, the considered propellant gas is Xenon, so all the parameters depending on the gas will be chosen as if Xenon was being used. It is the most used gas because it has a high atomic weight (higher energy for the same acceleration) and, as it is a noble gas, it is very stable and easy to store.

Before diving into the equations it is important to define some previous physic parameters that are useful to understand the equations.

6.1.1. Particle flow

For all means it is important to know the amount of particles that cross a surface in a unit of time. So the particle flow for any species is defined as the product of the density of particles and the velocity of the mentioned particles, obtaining the desired units of $\frac{particles}{m^2 s}$.

For electrons, ions and neutrals the particle flows read

$$\Gamma_e = n_e v_e \quad (49)$$

$$\Gamma_i = n_i v_i \cong n_e v_i \quad (50)$$

$$\Gamma_n = n_n v_n \quad (51)$$

Where n refers to the density of particles and v the velocity. It is important to know that the velocity of the neutrals is constant and, in the case of Xenon, equal to 300 meters per second.

6.1.2. Frequencies of creation and collisions

Ions are created all along the channel by collisions of neutrals and electrons. The rate at which this happens can be quantified and it is called ions creation frequency. It follows the expression below.

$$v_{ion} = n_n R_i \tag{52}$$

Where R_i is experimentally found to be

$$R_i = \sigma_o \bar{c_e} \left(1 + 2\frac{kT_e}{E_i}\right) e^{-\frac{E_i}{kT_e}} \tag{53}$$

Where σ_o is a characteristic surface, k is the Boltzmann constant, E_i is the energy needed for ionization (in the case of Xenon $\sigma_o = 3.6 \times 10^{-20}\, m^2$, $k = 1.38095 \times 10^{-23} \frac{J}{K}$, $E_i = 12.1e\ J$), T_e is the temperature of electrons and $\bar{c_e}$ is the mean temperature velocity of the electrons that has the following expression found experimentally.

$$\bar{c_e} = \sqrt{\frac{8}{\pi}\frac{kT_e}{m_i}} \tag{54}$$

Where $m_i = 2.2 \times 10^{-25}\, kg$ is the mass of the ion of Xenon.

However, for computation effects, the frequency of ionization is not exactly the same as the frequency of impacts between neutrals and electrons. The expression for the frequency of neutrals and electrons collisions is

$$v_{en} = n_n \bar{c_e} \sigma_{en} \tag{55}$$

Where a new effective collision surface appears that, for the case of Xenon, is $\sigma_{en} = 27 \times 10^{-20}\, m^2$.

6.2. Ion and electron mass equation

To obtain the mass equation it is important to evaluate the creation of particles in every position along the channel. To do so, it is considered a differential control volume where the flow of ions is increased by a differential part. The graphical definition of the mentioned volume can be seen below.

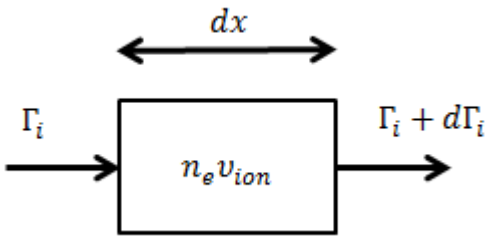

Figure 19: **Control volume considered**

Remembering the meaning of Γ_i with equation **(50)**, it can be easily affirmed that in a space dx the flow of ions increases a quantity $d\Gamma_i$ thanks to the contribution of the effect $n_e v_{ion}$. Setting out the mass conservation inside this control volume.

$$A(\Gamma_i + d\Gamma_i) - \Gamma_i A = n_e v_{ion} A dx$$

Where the transversal area term A can be simplified.

$$\Gamma_i - \Gamma_i + d\Gamma_i = n_e v_{ion} dx$$

Finally the relation obtained is

$$\frac{d\Gamma_i}{dx} = n_e v_{ion} \qquad (56)$$

Notice now that, as it has been explained before, the creation of an ion is intrinsic to the release of an electron and so, the disappearance of a neutral, thus

$$\frac{d\Gamma_i}{dx} = \frac{d\Gamma_e}{dx} = -\frac{d\Gamma_n}{dx} \qquad (57)$$

Using equations **(56)** and **(57)**, the mass conservation equation is found.

$$\frac{d\Gamma_i}{dx} = \frac{d\Gamma_e}{dx} = -\frac{d\Gamma_n}{dx} = n_e v_{ion} \qquad (58)$$

However, some extra information can be obtained by integrating two parts of the previous equation.

$$\frac{d}{dx}(\Gamma_i + \Gamma_n) = 0 \quad \Rightarrow \quad \Gamma_i + \Gamma_n = C_1$$

$$\frac{d}{dx}(\Gamma_i - \Gamma_e) = 0 \quad \Rightarrow \quad \Gamma_i - \Gamma_e = C_2$$

Where C_1 and C_2 are constants that are defined as two constant flowes in determined Hall thruster Γ_m and Γ_d respectively. The value of these constants can be determined using the boundary conditions.

$$A(\Gamma_i - \Gamma_e)e = I_a \qquad (59)$$

$$A(\Gamma_i + \Gamma_n)m_i = \dot{m} \qquad (60)$$

The following relations are obtained.

$$\Gamma_i + \Gamma_n = \Gamma_m = \frac{\dot{m}}{Am_i} \quad (61)$$

$$\Gamma_i - \Gamma_e = \Gamma_d = \frac{I_a}{Ae} \quad (62)$$

Where $\dot{m}$, A,m_i, I_a and e are the usual variables that have been used before.

6.3. Ion momentum equation

Similarly as before, to obtain the desired equation a control volume needs to be implemented. The difference is that, in this case, only the elements that are treated as particles are considered, that is the ions and neutrals.

So the control volume is as follows.

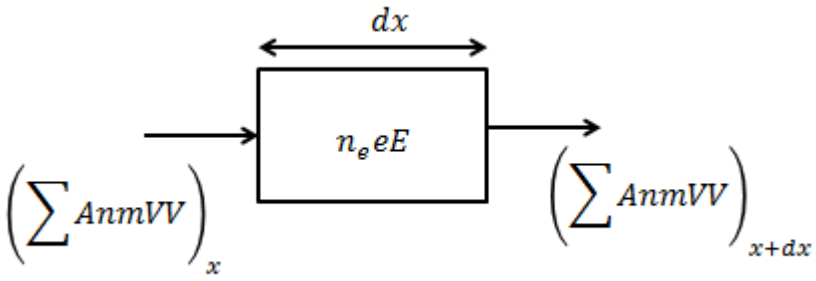

Figure 20: **Control volume considered**

The variation of momentum in heavy particles in a differential space dx is only due to the contribution of the electrical field per unit volume $n_e eE$.

So, writing the equilibrium of momentum in the control volume and distinguishing between neutrals and ions.

$$(Anmvv)_{x+dx}^{ions} + (Anmvv)_{x+dx}^{neutrals} - (Anmvv)_{x}^{ions} - (Anmvv)_{x}^{neutrals} = Adxn_e eE$$

Breaking down the terms and simplifying.

$$\frac{d}{dx}(An_i m_i v_i v_i)dx + \frac{d}{dx}(An_n m_i v_n v_n)dx = An_e eEdx$$

At this point, it is important to remember the definition **(50)** that stablishes $\Gamma = nv$, and the equivalence previously demonstrated $n_e = n_i$.

Using these two relations and working on the mathematics it is obtained

$$m_i \frac{d}{dx}(\Gamma_i v_i) + m_i \frac{d}{dx}(\Gamma_n v_n) = n_e eE$$

Differentiating

$$m_i \left(\frac{d\Gamma_i}{dx} v_i + \Gamma_i \frac{dv_i}{dx} + \frac{d\Gamma_n}{dx} v_n + \Gamma_n \frac{dv_n}{dx}\right) = n_e eE$$

Where the term $\Gamma_n \frac{dv_n}{dx}$ can be eliminated because the velocity of the neutrals, that are not affected by neither the electrical or magnetic fields, does not change throughout the channel $\left(\frac{dv_n}{dx} \approx 0\right)$. In addition, applying the mass conservation equation **(57)**, the term $\frac{d\Gamma_n}{dx}$ can be substituted by the more suitable term of $-\frac{d\Gamma_i}{dx}$.

Continuing with mathematical work on the equation.

$$m_i \frac{d\Gamma_i}{dx}(v_i - v_n) + m_i \Gamma_i \frac{dv_i}{dx} = n_e e E$$

Again, with the help of mass conservation equation **(58)**.

$$m_i n_e v_{ion}(v_i - v_n) + m_i n_e v_i \frac{dv_i}{dx} = n_e e E$$

After the final simplifying step, the ion momentum equation is obtained.

$$m_i v_i \frac{dv_i}{dx} = eE - m_i v_{ion}(v_i - v_n) \qquad (63)$$

Observing the equation, it is clear that the ion momentum term $\left(m_i v_i \frac{dv_i}{dx}\right)$ changes not only by the contribution of the electrical field (eE), but also has a negative contribution $\left(m_i v_{ion}(v_i - v_n)\right)$. This negative contribution can be understood as a kind of drag, meaning that it diminishes the increase of momentum, caused by the ionization of neutrals. Every time a particle is ionized, a new ion is incorporated to the terms that consider ions' behavior jumping from the neutral velocity to a higher ion velocity and generating the mentioned negative term.

6.4. Electron momentum equation

Unlike the sections above, electrons are treated now. So we are talking about a fluid now, not particles. This fact changes the approach to the final equation.

As fluid is being treated, it is useful to redefine to axis that will be used later on. Following Martínez-Sánchez lead, these axis are defined in the figure below.

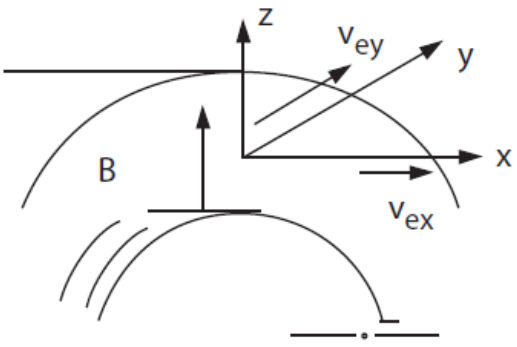

Figure 21: **Axis defined (Martínez Sánchez)**

Considering only classical electron collisions (with neutrals only), electrical and magnetic forces and the negative effect caused by collisions the vector Navier-Stokes equation adapted to the situation can be formulated.

$$\nabla P_e = -en_e\left(\vec{E} + \overrightarrow{v_e} \times \vec{B}\right) - m_e \upsilon_{en} n_e \overrightarrow{v_e} \quad (64)$$

Where υ_{en} is the frequency of collisions between neutrals and electrons that has been defined before.

What the equation basically says is that the variation of pressure of the electrons in any of the three defined directions depends not only on the contribution of the electrical and magnetic field $\left(-en_e\left(\vec{E} + \overrightarrow{v_e} \times \vec{B}\right)\right)$, but also has a negative contribution caused by the collisions between neutrals and electrons $(-m_e \upsilon_{en} n_e \overrightarrow{v_e})$.

Developing the product $\overrightarrow{v_e} \times \vec{B}$.

$$\begin{bmatrix} \vec{\imath} & \vec{\jmath} & \vec{k} \\ v_{ex} & v_{ey} & v_{ez} \\ 0 & 0 & B \end{bmatrix} = \begin{pmatrix} v_{ey}B \\ -v_{ex}B \\ 0 \end{pmatrix}$$

Distinguishing between x and y axis.

$$\frac{dP_e}{dx} = -en_e\left(E_x + v_{ey}B\right) - m_e \upsilon_{en} n_e v_{ex} \quad (65)$$

$$\frac{dP_e}{dy} = -en_e\left(E_y - v_{ex}B\right) - m_e \upsilon_{en} n_e v_{ey} \quad (66)$$

Notice that, as the model considered is an unidimensional one, the pressure of the electrons in the y direction remains constant, so $\frac{dP_e}{dy} \approx 0$. In addition, the electrical field was defined in the longitudinal direction (following x axis) so there is no electrical field in the y direction $(E_y \approx 0)$.

Rewriting expression **(66)** (y axis).

$$0 = -e(0 - v_{ex}B) - m_e \upsilon_{en} v_{ey}$$

Isolating v_{ey}.

$$v_{ey} = \frac{eB}{m_e \upsilon_{en}} v_{ex}$$

Where the cyclotronic frequency **(25)** appears, leading to

$$v_{ey} = \frac{\omega_c}{\upsilon_{en}} v_{ex} \quad (67)$$

The previous relation between velocities in both axis is very useful because it can be substituted into equation **(65)**. Doing this

$$\frac{dP_e}{dx} = -en_e\left(E_x + \frac{\omega_c}{\upsilon_{en}}v_{ex}B\right) - m_e\upsilon_{en}n_ev_{ex}$$

Regrouping in useful terms and using relation **(25)** again $(eB = \omega_c m_e)$.

$$\frac{dP_e}{dx} = -en_eE_x - m_en_ev_{ex}\left(\frac{\omega_c^2}{\upsilon_{en}} + \upsilon_{en}\right)$$

As it has been explained multiple times, the main feature of a Hall thruster is that the electrons get trapped in a circular motion by the combination of an electrical and a magnetic field. According to that it is not absurd to think that an electron will complete lots of turns around the axis before colliding with a neutral. In this situation $\omega_c \gg \upsilon_{en}$, so

$$\frac{\omega_c^2}{\upsilon_{en}} + \upsilon_{en} \approx \frac{\omega_c^2}{\upsilon_{en}}$$

The obtained term acts as an "effective collision frequency" accounting for the magnetic effect.

$$\upsilon_e = \frac{\omega_c^2}{\upsilon_{en}} \quad (68)$$

If an expression for the pressure of the electrons needs to be written, the expression for ideal gases can be used.

$$P_e = n_ekT_e \quad (69)$$

Where k is the Boltzmann's constant again.

Resulting on the definitive form of the electron momentum equation.

$$\frac{d}{dx}(n_ekT_e) = -en_eE_x - m_en_ev_{ex}\upsilon_e \quad (70)$$

However, being rigorous, the expression found for the effective collision frequency is false.

In a Hall thruster the dominant scattering effect is not neutral-electron collisions, but the random deflections due to plasma turbulence.

In this situation where anomalous or Bohm diffusion dominates, it is empirically found (Ahedo & Martínez-Sánchez) that the expression for the effective collision frequency is

$$\upsilon_e = \frac{\omega_c^2}{\upsilon_{en} + \alpha_B\omega_c} \quad (71)$$

Where α_B is the Bohm parameter with a value experimentally found.

$$\alpha_B = \frac{1}{16} \quad (72)$$

For implementing the code, this last expression **(71)** will be used as it has a better level of precision.

6.5. Electron energy equation

To obtain the electron energy equation the previously used methodology of defining a control volume is followed. Remember that the equivalent expression for the ions will not be found because, as they are treated like particles, it will be redundant with the momentum equation.

The kinetic energy for an ideal gas

$$E_k = \frac{1}{2}mv^2 = \frac{3}{2}kT \qquad (73)$$

Thus, defining a control volume where the kinetic energy changes in a differential way

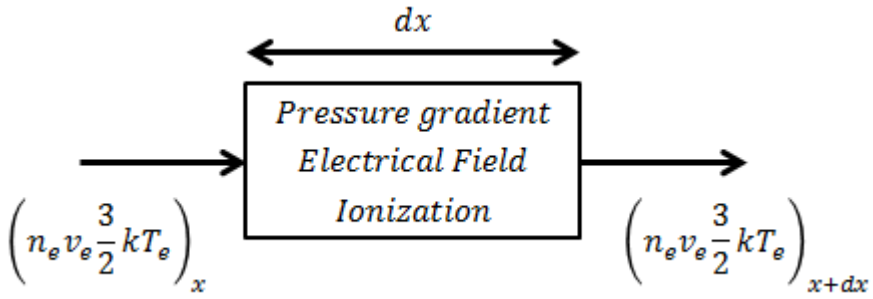

Figure 22: **Control volume considered**

The equilibrium of energy inside the control volume can be written considering the three aspects that make energy change: the pressure gradient, the electrical field and ionization of neutrals.

$$\left(An_e v_e \frac{3}{2} kT_e\right)_{x+dx} - \left(An_e v_e \frac{3}{2} kT_e\right)_x =$$

$$= (AP_e v_e)_x - (AP_e v_e)_{x+dx} - eEn_e v_e A dx - n_e \upsilon_{ion} E_i' A dx$$

Simplifying some terms and using equation **(69)** $(P_e = n_e kT_e)$.

$$\frac{d}{dx}\left(An_e v_e \frac{3}{2} kT_e\right) dx = -\frac{d}{dx}(An_e kT_e v_e) dx - eEn_e v_e A dx - n_e \upsilon_{ion} E_i' A dx$$

At this point A and dx can be eliminated and, using equation **(49)** $(\Gamma_e = n_e v_e)$, the expression above results

$$\frac{d}{dx}\left(\Gamma_e \frac{3}{2} kT_e\right) = -\frac{d}{dx}(\Gamma_e kT_e) - eE\Gamma_e - n_e \upsilon_{ion} E_i'$$

The previous expression tells that the variation of kinetic energy inside the volume of control has three main contributions:

- $-\frac{d}{dx}(\Gamma_e kT_e)$ is the term that takes into account the pressure gradient.
- $-eE\Gamma_e$ expresses the effect of the electrical field on the energy of electrons.
- $-n_e v_{ion} E_i'$ stands for the effect of ionization of neutrals inside the control volume, where E_i' is considered as 2.5 times the energy of ionization in order to include radiative losses due to excitation by electron impact, followed by photon emission. For the case considered of Xenon $E_i' = 2.5 \cdot 12.1\ eV = 30.25\ eV$.

Finally, the definitive form of the electron energy equation is

$$\frac{d}{dx}\left(\Gamma_e \frac{5}{2} kT_e\right) = -eE\Gamma_e - n_e v_{ion} E_i' \qquad (74)$$

With the electron energy equation, all the expressions needed for the unidimensional model have been obtained.

6.6. Obtaining the differential equations

Before starting to solve the system, equations **(58)**, **(63)**, **(70)** and **(74)** that form it are combined for clarity.

$$\frac{d}{dx}(n_e v_i) = n_e v_{ion}$$

$$m_i v_i \frac{dv_i}{dx} - eE_x = -m_i \nu_{ion}(v_i - v_n)$$

$$kT_e \frac{dn_e}{dx} + kn_e \frac{dT_e}{dx} + en_e E_x = -m_e n_e \nu_{ex} \nu_e$$

$$\frac{d}{dx}\left[\Gamma_e \left(\frac{5}{2} kT_e + E_i'\right)\right] = -e\Gamma_e E_x$$

It is a complicated system and needs work on the mathematics. The first step is to write it on matrix form taking into consideration that $E_x = -\frac{d\phi}{dx}$.

$$\begin{bmatrix} n_e & v_i & 0 & 0 \\ m_i v_i & 0 & 0 & e \\ 0 & kT_e & kn_e & -en_e \\ 0 & 0 & k(5/2)\Gamma_e & -e\Gamma_e \end{bmatrix} \begin{bmatrix} dv_i/dx \\ dn_e/dx \\ dT_e/dx \\ d\phi/dx \end{bmatrix} = \begin{bmatrix} n_e \nu_{ion} \\ -m_i \nu_{ion}(v_i - v_n) \\ -m_e n_e \nu_{ex} \nu_e \\ -n_e \nu_{ion}\left(\frac{5}{2} kT_e + E_i'\right) \end{bmatrix}$$

This system has the form $AX = B$, where

$$A = \begin{bmatrix} n_e & v_i & 0 & 0 \\ m_i v_i & 0 & 0 & e \\ 0 & kT_e & kn_e & -en_e \\ 0 & 0 & k(5/2)\Gamma_e & -e\Gamma_e \end{bmatrix}$$

$$B = \begin{bmatrix} n_e \nu_{ion} \\ -m_i \nu_{ion}(v_i - v_n) \\ -m_e n_e v_{ex} \nu_e \\ -n_e \nu_{ion}\left(\frac{5}{2}kT_e + E_i'\right) \end{bmatrix}$$

$$X = \begin{bmatrix} dv_i/dx \\ dn_e/dx \\ dT_e/dx \\ d\phi/dx \end{bmatrix}$$

To solve it, it is indispensable to isolate X, so the form $X = A^{-1}B$ is needed.

Next step is, then, calculating the inverse matrix of A. To do so, the determinant of A is needed.

$$D = n_e e k^2 (5/2)\Gamma_e T_e - (3/2) k n_e e \Gamma_e m_i v_i^2 = (3/2) k n_e e \Gamma_e \left[(5/3)kT_e - m_i v_i^2\right]$$

And so it is the adjunct of the transposed matrix.

$$A^{-T} = \frac{1}{D}\begin{bmatrix} ek^2\left(\frac{5}{2}\right)\Gamma_e T_e & -v_i k\left(\frac{3}{2}\right)\Gamma_e e n_e & -v_i k\left(\frac{5}{2}\right)\Gamma_e e & v_i k n_e e \\ -\left(\frac{3}{2}\right) k n_e e \Gamma_e m_i v_i & e n_e^2 k\left(\frac{3}{2}\right)\Gamma_e & n_e k\left(\frac{5}{2}\right)\Gamma_e e & -n_e^2 k e \\ -m_i v_i k T_e e \Gamma_e & e n_e k T_e \Gamma_e & e\Gamma_e m_i v_i^2 & e n_e\left(kT_e - m_i v_i^2\right) \\ -m_i v_i k^2 T_e\left(\frac{5}{2}\right)\Gamma_e & n_e k^2\left(\frac{5}{2}\right) T_e \Gamma_e & m_i v_i^2 k\left(\frac{5}{2}\right)\Gamma_e & -k n_e m_i v_i^2 \end{bmatrix}$$

Now that the unknowns are isolated, the equation can be written back to separate form.

$$\left[\frac{5}{3}kT_e - m_i v_i^2\right]\frac{dv_i}{dx} = \frac{ek^2(5/2)\Gamma_e T_e n_e \nu_{ion}}{(3/2)kn_e e\Gamma_e} + \frac{v_i k(3/2)\Gamma_e e n_e m_i \nu_{ion}(v_i - v_n)}{(3/2)kn_e e\Gamma_e} + \frac{v_i k(5/2)\Gamma_e e m_e n_e v_{ex}\nu_e}{(3/2)kn_e e\Gamma_e} - \frac{v_i k n_e e n_e \nu_{ion}\left(\frac{5}{2}kT_e + E_i'\right)}{(3/2)kn_e e\Gamma_e} \quad (75)$$

$$\left[\frac{5}{3}kT_e - m_i v_i^2\right]\frac{dn_e}{dx} = -\frac{(3/2)kn_e e\Gamma_e m_i v_i n_e \nu_{ion}}{(3/2)kn_e e\Gamma_e} - \frac{en_e^2 k(3/2)\Gamma_e m_i \nu_{ion}(v_i - v_n)}{(3/2)kn_e e\Gamma_e} - \frac{n_e k(5/2)\Gamma_e e m_e n_e v_{ex}\nu_e}{(3/2)kn_e e\Gamma_e} + \frac{n_e^2 k e n_e \nu_{ion}\left(\frac{5}{2}kT_e + E_i'\right)}{(3/2)kn_e e\Gamma_e} \quad (76)$$

$$\left[\frac{5}{3}kT_e - m_i v_i^2\right]\frac{dT_e}{dx} = -\frac{m_i v_i kT_e e\Gamma_e n_e \nu_{ion}}{(3/2)kn_e e\Gamma_e} - \frac{en_e kT_e \Gamma_e m_i \nu_{ion}(v_i - v_n)}{(3/2)kn_e e\Gamma_e} - \frac{e\Gamma_e m_i v_i^2 m_e n_e v_{ex} \nu_e}{(3/2)kn_e e\Gamma_e} - \frac{en_e\left(kT_e - m_i v_i^2\right)n_e \nu_{ion}\left(\frac{5}{2}kT_e + E_i'\right)}{(3/2)kn_e e\Gamma_e} \quad (77)$$

$$\left[\frac{5}{3}kT_e - m_i v_i^2\right]\frac{d\phi}{dx} = -\frac{m_i v_i k^2 T_e (5/2)\Gamma_e n_e \nu_{ion}}{(3/2)kn_e e\Gamma_e} - \frac{n_e k^2 (5/2)T_e \Gamma_e m_i \nu_{ion}(v_i - v_n)}{(3/2)kn_e e\Gamma_e} - \frac{m_e n_e v_{ex} \nu_e m_i v_i^2 k(5/2)\Gamma_e}{(3/2)kn_e e\Gamma_e} + \frac{kn_e m_i v_i^2 n_e \nu_{ion}\left(\frac{5}{2}kT_e + E_i'\right)}{(3/2)kn_e e\Gamma_e} \quad (78)$$

These expressions are still too heavy, mathematical work can be performed to obtain simpler equations. However, the procedure has not been included not to make the lecture tedious.

The final expressions obtained are

$$\left[\frac{5}{3}kT_e - m_i v_i^2\right]\frac{dv_i}{dx} = = \frac{5}{3}m_e \nu_e \nu_e v_i + \nu_{ion}\left[\frac{5}{3}kT_e + m_i v_i(v_i - v_n) - v_i\left(\frac{2E_i' + 5kT_e}{3v_e}\right)\right] \quad (79)$$

$$\left[\frac{5}{3}kT_e - m_i v_i^2\right]\frac{dn_e}{dx} = = -\frac{5}{3}m_e n_e \nu_e \nu_e - n_e \nu_{ion}\left[m_i(2v_i - v_n) - \frac{2E_i' + 5kT_e}{3v_e}\right] \quad (80)$$

$$\left[\frac{5}{3}kT_e - m_i v_i^2\right]k\frac{dT_e}{dx} = = -\frac{2}{3}m_i v_i^2 m_e \nu_e \nu_e - m_i \nu_{ion}\left[\frac{2}{3}kT_e(2v_i - v_n) - \frac{m_i v_i^2 - kT_e}{m_i}\frac{2E_i' + 5kT_e}{3v_e}\right] \quad (81)$$

$$\left[\frac{5}{3}kT_e - m_i v_i^2\right]e\frac{d\phi}{dx} = = -\frac{5}{3}m_e \nu_e \nu_e m_i v_i^2 - m_i \nu_{ion}\left[\frac{5}{3}kT_e(2v_i - v_n) - v_i^2\left(\frac{2E_i' + 5kT_e}{3v_e}\right)\right] \quad (82)$$

This differential equations' system can be solved for every position along the cannel in Matlab using "ode" solver, indeed, the necessary code was written and presented some problems. Sometimes the great discrepancy in the magnitude order of the different variables produces a loss of consistency in the resolution of the system, presenting non expected and erroneous solutions.

To fix the trouble, the previous equations (79), (80), (81) and (82) can be nondimensionalized.

6.7. Nondimensionalization

The method of nondimensionalization followed is the one proposed by Professor Ahedo and Professor Martínez-Sánchez in their article *One Dimensional Plasma Structure in Hall Thrusters* (Ahedo & Martínez-Sánchez).

6.7.1. Characteristic parameters

The first step of the nondimensionalization is defining the characteristic parameters that will permit performing it.

There are three parameters that need to be given an arbitrary value; a characteristics length, surface and energy.

$$l^* = 0.01\ m$$

$$T^* = E_i = 1.9384 \cdot 10^{-18}\ J$$

$$\sigma^* = \sigma_o \sqrt{\frac{m_i}{m_e}} = 1.8 \cdot 10^{-17}\ m^2$$

With these three parameters it is possible to nondimensionalize all the equations. All the other characteristic parameters can be obtained from the previous three.

$$v^* = \sqrt{\frac{T^*}{m_i}} = 2345\ m/s$$

$$n^* = \frac{1}{\sigma^* l^*} = 5.56 \cdot 10^{18}\ m^{-3}$$

$$\Gamma^* = n^* v^* = 1.3 \cdot 10^{22}\ m^{-2} s^{-1}$$

$$v^* = \frac{v^*}{l^*} = 2.35 \cdot 10^{5}\ s^{-1}$$

6.7.2. Main equations nondimensionalization

As the nondimensionalization process is the same for all the four equations, it will only be shown for the first one, the three remaining will be written directly on its nondimensional form to avoid being tedious.

Starting with equation **(79)**,five terms are defined for convenience on nondimensionalization.

$$\underbrace{\left[\frac{5}{3}kT_e - m_i v_i^2\right]\frac{dv_i}{dx}}_{1} = \underbrace{\frac{5}{3}m_e v_e \nu_e v_i}_{2} + \nu_{ion}\left[\underbrace{\frac{5}{3}kT_e}_{3} + \underbrace{m_i v_i (v_i - v_n)}_{4} - \underbrace{v_i\left(\frac{2E_i' + 5kT_e}{3v_e}\right)}_{5}\right]$$

Beginning nondimensionalization with term 1

$$\left[\frac{5}{3}kT_e - m_i v_i^2\right]\frac{dv_i}{dx} = \left[\frac{5}{3}\tilde{T}_e T^* - m_i \tilde{v}_i^{\,2} v^{*2}\right]\frac{d\tilde{v}_i v^*}{d\tilde{x} l^*} = (T^* v^*)\left[\frac{5}{3}\tilde{T}_e - \tilde{v}_i^{\,2}\right]\frac{d\tilde{v}_i}{d\tilde{x}}$$

Jumping now to term 2

$$\frac{5}{3}m_e v_e \nu_e v_i = \frac{5}{3}\widetilde{m_e} m_i \widetilde{v_e} v^* \tilde{\nu}_e v^* \tilde{v}_i v^* = (T^* v^*)\frac{5}{3}\widetilde{m_e}\widetilde{v_e}\tilde{\nu}_e\tilde{v}_i$$

Regarding term 3

$$\nu_{ion}\frac{5}{3}kT_e = \frac{5}{3}\tilde{\nu}_{ion} v^* \tilde{T}_e T^* = (T^* v^*)\frac{5}{3}\tilde{\nu}_{ion}\tilde{T}_e$$

Again, the same procedure for term 4

$$\nu_{ion} m_i v_i (v_i - v_n) = \tilde{\nu}_{ion} v^* m_i \tilde{v}_i v^* (\tilde{v}_i - \widetilde{v_n}) v^* = (T^* v^*)\tilde{\nu}_{ion}\tilde{v}_i(\tilde{v}_i - \widetilde{v_n})$$

Finally, for the term 5

$$v_i \nu_{ion}\left(\frac{2E_i' + 5kT_e}{3\nu_e}\right) = \tilde{v}_i v^* \tilde{\nu}_{ion} v^*\left(\frac{2\widetilde{E_i'}T^* + 5\tilde{T}_e T^*}{3\widetilde{\nu_e} v^*}\right) = (T^* v^*)\tilde{v}_i\tilde{\nu}_{ion}\left(\frac{2\widetilde{E_i'} + 5\tilde{T}_e}{3\widetilde{\nu_e}}\right)$$

Notice that all the nondimensionalized terms include the factor $(T^* v^*)$, so the final nondimensional form of the equation (79)

$$\left[\frac{5}{3}\tilde{T}_e - \tilde{v}_i^{\,2}\right]\frac{d\tilde{v}_i}{d\tilde{x}} = \frac{5}{3}\widetilde{m_e}\widetilde{v_e}\tilde{\nu}_e\tilde{v}_i + \tilde{\nu}_{ion}\left[\frac{5}{3}\tilde{T}_e + \tilde{v}_i(\tilde{v}_i - \widetilde{v_n}) - \tilde{v}_i\left(\frac{2\widetilde{E_i'} + 5\tilde{T}_e}{3\widetilde{\nu_e}}\right)\right] \qquad (83)$$

To reduce computational effort some factors that, as it will be seen, are common in all the expressions, are defined in order to be precalculated and so, for every step, they will be calculated just once instead of four times.

The common parts are

$$(denom) = \frac{5}{3}\tilde{T}_e - \tilde{v}_i^{\,2} \qquad (84)$$

$$K_1 = \frac{\widetilde{m_e}\widetilde{v_e}\tilde{\nu}_e}{3} \qquad (85)$$

$$K_2 = \frac{2\widetilde{E_i'} + 5\tilde{T}_e}{3\widetilde{\nu_e}} \qquad (86)$$

So equation **(83)** can be rewritten.

$$(\text{denom})\frac{d\tilde{v}_i}{d\tilde{x}} = 5\mathrm{K}_1\tilde{v}_i + \tilde{\nu}_{ion}\left[\frac{5}{3}\tilde{T}_e + \tilde{v}_i(\tilde{v}_i - \widetilde{v_n}) - \tilde{v}_i\mathrm{K}_2\right] \qquad (87)$$

Following the same procedure, equations **(80)**, **(81)** and **(82)** can be rewritten in nondimensional form.

$$(\text{denom})\frac{d\widetilde{n_e}}{d\tilde{x}} = -5\mathrm{K}_1\widetilde{\nu_e} - \widetilde{n_e}\tilde{\nu}_{ion}[2\tilde{v}_i - \widetilde{v_n} - \mathrm{K}_2] \qquad (88)$$

$$(\text{denom})\frac{d\widetilde{T_e}}{d\tilde{x}} = -2\mathrm{K}_1\widetilde{v_i}^2 - \tilde{\nu}_{ion}\left[\frac{2}{3}\widetilde{T_e}(2\widetilde{v_i} - \widetilde{v_n}) - (\widetilde{v_i}^2 - \widetilde{T_e})\mathrm{K}_2\right] \quad (89)$$

$$(\text{denom})\frac{d\tilde{\phi}}{d\tilde{x}} = 5\mathrm{K}_1\widetilde{v_i}^2 + \tilde{\nu}_{ion}\left[\frac{5}{3}\widetilde{T_e}(2\widetilde{v_i} - \widetilde{v_n}) - \widetilde{v_i}^2\mathrm{K}_2\right] \quad (90)$$

Once the nondimensional expressions are obtained, it is time to find the nondimensional parameters that appear in them.

6.7.3. Secondary parameters nondimensionalization

The procedure for nondimensionalising the parameters in this subsection is the same that for the main equations. So the goal of the text is not to show how the parameters are nondimensionalized but to write the final forms of the nondimensional parameters.

In one hand, there are the different nondimensional frequencies.

The ion creation frequency

$$\tilde{\nu}_{ion} = \widetilde{n_n}\tilde{\sigma}_o\sqrt{\frac{8\widetilde{T_e}}{\pi}}\left(1 + 2\frac{\widetilde{T_e}}{\widetilde{E_i}}\right)e^{-\frac{\widetilde{E_i}}{\widetilde{T_e}}} \quad (91)$$

The electron-neutral collision frequency

$$\tilde{\upsilon}_{en} = \widetilde{n_n}\tilde{\sigma}_{en}\sqrt{\frac{8\widetilde{T_e}}{\pi}} \quad (92)$$

And finally, the effective collision frequency

$$\widetilde{\upsilon_e} = \frac{\widetilde{\omega_c}}{\tilde{\upsilon}_{en} + \alpha_B\widetilde{\omega_c}} \quad (93)$$

Then, the nondimensional electron velocity is also essential

$$\widetilde{v_e} = \frac{\widetilde{\Gamma_e}}{\widetilde{n_e}} \quad (94)$$

The density of neutrals

$$\widetilde{n_n} = \frac{\widetilde{\Gamma_n}}{\widetilde{v_n}} \quad (95)$$

Of course, the three particle flows

$$\widetilde{\Gamma_n} = \widetilde{\Gamma_m} - \widetilde{\Gamma_i} \quad (96)$$

$$\widetilde{\Gamma_e} = \widetilde{\Gamma_i} - \widetilde{\Gamma_d} \quad (97)$$

$$\widetilde{\Gamma_i} = \widetilde{n_e}\widetilde{v_i} \quad (98)$$

And the last one, the cyclotronic frequency

$$\widetilde{\omega_c} = \frac{eB}{m_e v^*} \quad (99)$$

All the other nondimensional factors that appear and are not clearly defined in this subsection are considered design parameters and calculated simply taking the dimensional value and dividing it by the convenient characteristic parameter.

6.8. Boundary conditions

It is essential to study the singularities of the equations describing the different parameters. The most important feature is that the common denominator in the equations can be zero, creating a special point out of the domain.

$$\frac{5}{3} kT_e - m_i v_i^2 = 0$$

What happens when the ions have a velocity of

$$v_{is} = \sqrt{\frac{5}{3}\frac{kT_e}{m_i}} \quad (100)$$

Which is the ion-sonic wave speed, meaning that when the ions reach this velocity, an acoustic wave is created in which both ions and electrons undergo compressions and expansions. It is important to notice that both electrons and ions have contributions in the expression above, which is not absurd to think because they are coupled to each other electrostatically.

The only situation considered in this study is a case where this sonic situation is achieved at the open-end of the channel, just like a normal open gas pipe discharging into vacuum. With this assumption, the end condition is imposed in terms of that the velocity at the end must be v_{is}. The acceleration across this limit velocity is abrupt.

Another possible situation, which is not studied in the document but left for further future studies, is the case when the acoustic wave is situated inside the channel. This transition needs to be smooth and it happens when both sides of the equation are null. It is a complicated situation difficult to integrate.

However, apart from the "positive" acoustic wave, the sonic condition can be reached also at the anode $(x = 0)$. The model proposed (Ahedo & Martínez-Sánchez) considers that the anode creates a magnetic electron repelling sheath in order to restrict the electron capture. This sheath also attracts ions that, following the Bohm's criterion, will enter it at sonic velocity. Leaving to the condition

$$v_i(x = 0) = -\sqrt{\frac{5}{3}\frac{kT_e}{m_i}} = -v_{is} \quad (101)$$

To sum up, the model considered of Hall thruster has fixed inlet and exit velocities. It has a reversed sonic point at the anode and an abrupt sonic point at the exit.

In addition, equations **(80)** and **(81)** provide to extra boundary conditions by fixing to constant values.

$$\Gamma_m = \frac{\dot{m}}{Am_i}$$

$$\Gamma_d = \frac{I_a}{Ae}$$

Also initial values of T_e and n_e are indispensable.

6.9. Results using differential equations

Considering all the information given, the final distribution of the parameters along the channel can be now obtained.

The final obtained for an electrons' temperature at the inlet of $T_{e_o} = 0.1T^*$ graphs are

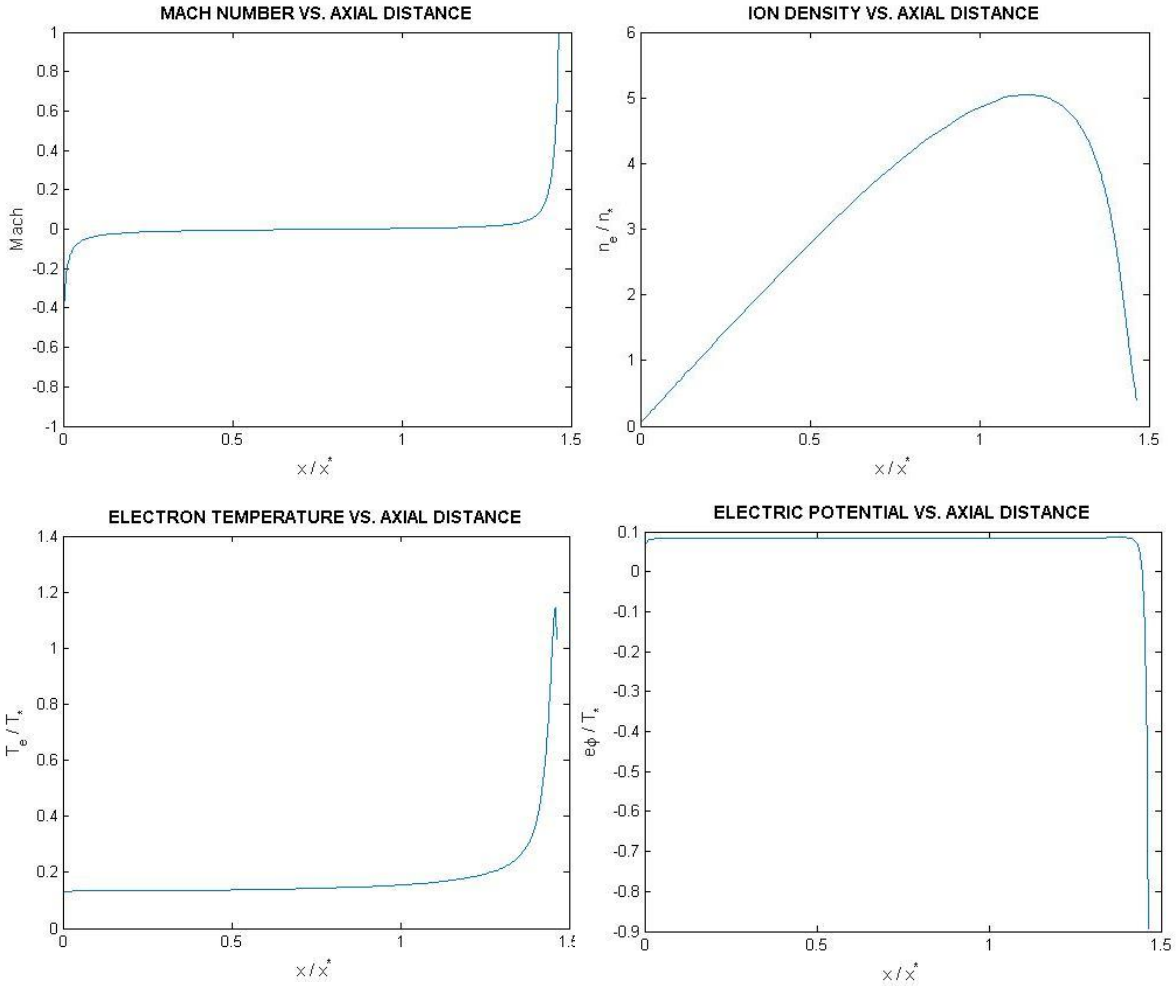

Figure 23. **Plasma variables for a channel with chocked exit, no wall losses and uniform magnetic field with $\frac{\Gamma_d}{\Gamma_m} = 1, T_{e_o} = 0.1T^*, \Gamma_{i_o} = -0.01\Gamma_m$**

It is important to mention, before analyzing the graphs, that neglecting wall loses and the two-dimensional effects can affect the distribution of the variables and slightly distance them from reality. In addition, the fact that the plume is neglected, makes that the behavior of the parameters at the very late channel is not strictly accurate. Even though, the one-dimensional model is a good approximation for a preliminary analysis.

Comparing the results with other one-dimensional models (Ahedo & Martínez-Sánchez) (Dan Goebel, 2008) and experimental analysis (Pote & Tedrake) (Haas, Gulczinski III, & Gallimore) one realizes the tendency of the variables is suitable to the expected but presents some punctual discrepancies.

To evaluate understand the behavior it is easier to analyze the variables separately.

In the case of the Mach, it starts with a reverse sonic point in order to accomplish the boundary Bohm condition given and this backwards velocity becomes smaller in modulus along the initial part of the channel. This velocity becomes lightly positive before the great acceleration produced by the presence of a higher electrical field. Then, the exit condition is also accomplished, as the beam exits the channel at sonic speed.

Therefore refers the electrons' density, the behavior is nearly the same as the obtained by other one-dimensional models. In the first regions the density increases tending to a straight line, what makes sense because, without this density gradient, the ions would have to advance towards he anode to maintain neutrality, something impossible due to the weakness of the electrical field in the zone. Once the density of electrons reaches a maximum it rapidly decays as expected when the ions are highly accelerated. It falls at the ionization zone to a low value, the density of electrons at the exit.

When analyzing the electrons temperature one notices that its behavior is also very similar to the presented in other articles. The temperature is low until it has a great grow.

To understand why the electrons' temperature has this distribution is better to analyze the channel from the exit to the end. At the exit of the channel, the backstream electrons have high energies because they have just been emitted by the cathode. Then there is a great loss of energy by ionization of the Xenon atoms at the final part of the channel, where most of the ionization occurs. From that point to the anode the energy, and so the temperature, remains low.

Finally, studying the plot of the distribution along the channel of ϕ, it can be realized that not only it is similar to other results, but also is in perfect accordance with the distribution of velocity. During the low ionization zone, the electrical field

remains very low. But when ionization happens, ϕ decreases rapidly, so, remembering that $E_x = -\frac{d\phi}{dx}$, the electrical field grows to a high positive value accelerating the ions created to the exit of the channel where they reach sonic velocities.

Another useful variable apart from the four presented above, is the evolution of the flow of ions along the channel. The figure below shows how this variable evolves.

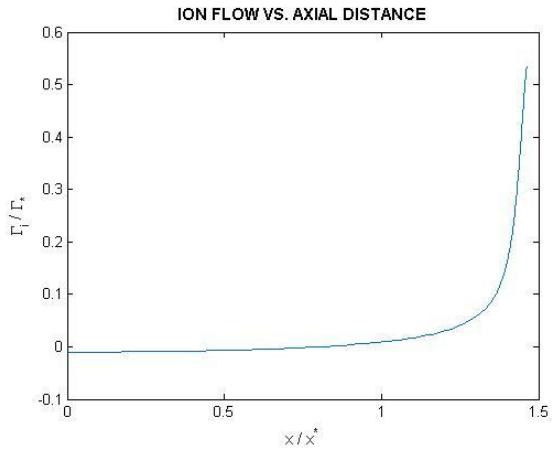

Figure 24. **Variation of ions' flow along a channel with $\frac{\Gamma_d}{\Gamma_m} = 1, T_{e_o} = 0.1T^*, \Gamma_{i_o} = -0.01\Gamma_m$**

The flow at the early stages of the channel is low, because ionization and acceleration of ions are nearly inexistent, but at the ionization zone, where ionization happens and the electrical field grows (accelerates the ions) the ion flow also grows as expected.

The results are quite accurate and permit studying perfectly what happens inside a Hall thruster.

However, to guarantee the correctness of the plots obtained, a specific study of the different zones found inside the channel is going to be done in the following chapter.

6.10. Variation with initial conditions

Before studying the approximations for different zones of the channel, numerical results have been obtained for different input parameters in order to verify the correct behavior of the code and its concordance with physical properties.

The only parameter that has been changed is the electrons temperature at the inlet T_{e_o}, so the energy of the beam was changed. The results obtained can be seen below.

T_{e_o} has always been expressed as a function of T^*.

For the case of $T_{e_o} = 0.15T^*$ the variables behaved as can be seen in the figure below.

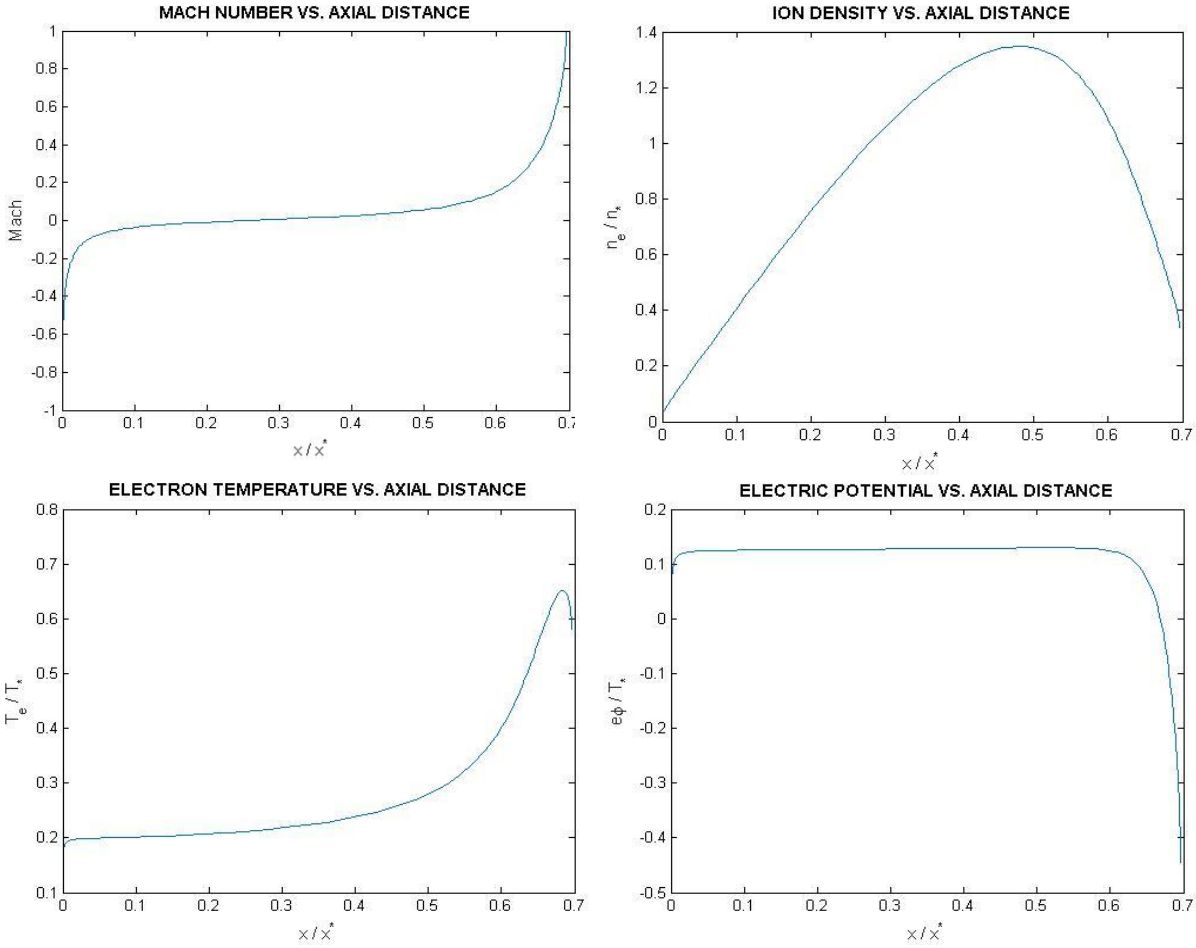

Figure 25. **Plasma variables for a channel with chocked exit, no wall losses and uniform magnetic field with $\frac{\Gamma_d}{\Gamma_m} = 1$, $T_{e_o} = 0.15T^*$, $\Gamma_{i_o} = -0.01\Gamma_m$**

And the ion's flow

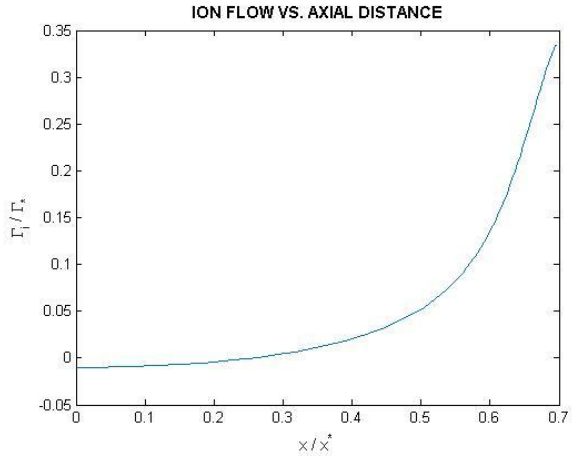

Figure 26. **Variation of ions' flow along a channel with $\frac{\Gamma_d}{\Gamma_m} = 1$, $T_{e_o} = 0.15T^*$, $\Gamma_{i_o} = -0.01\Gamma_m$**

The same can be done for an initial temperature of $T_{e_o} = 0.20T^*$

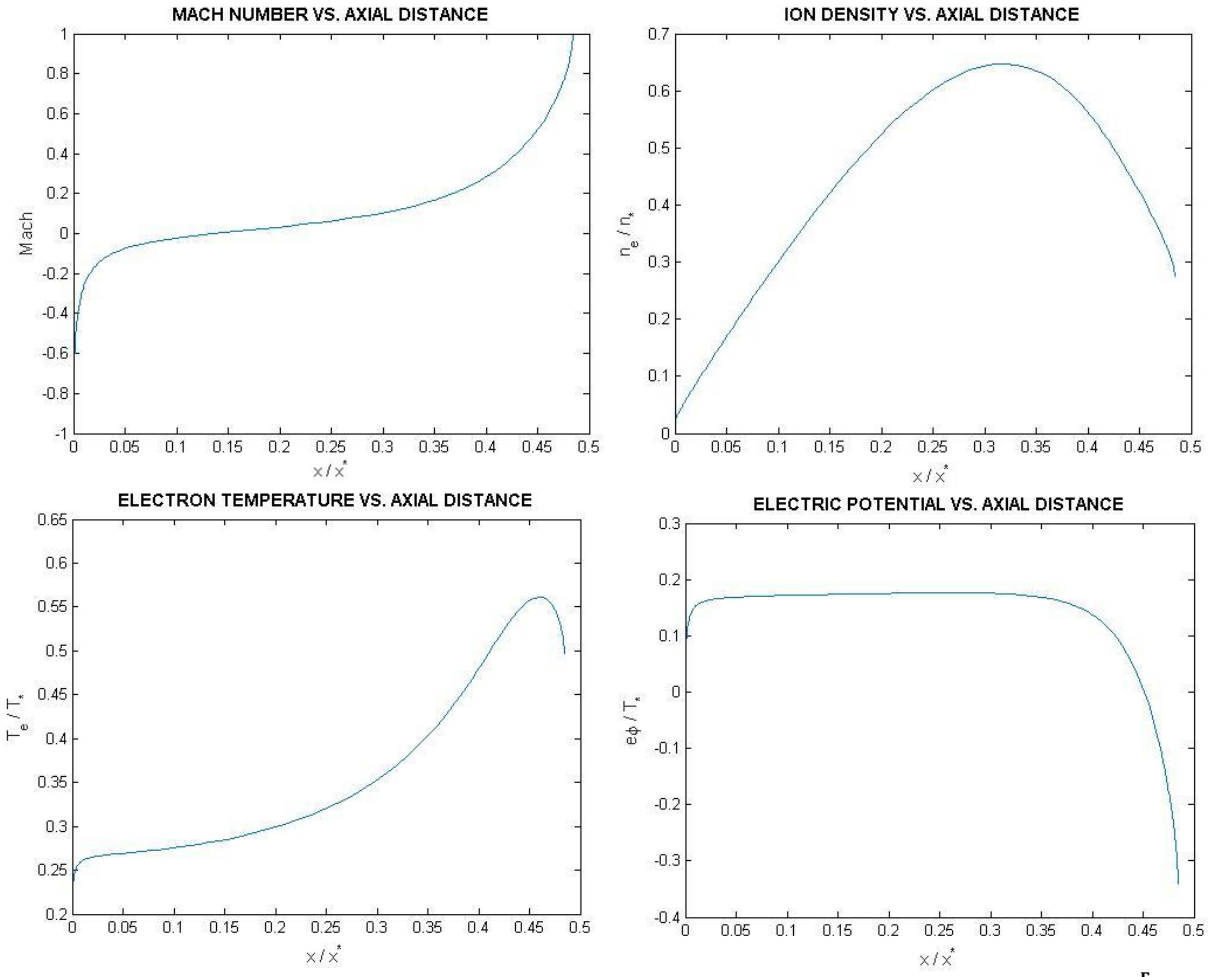

Figure 27. **Plasma variables for a channel with chocked exit, no wall losses and uniform magnetic field with $\frac{\Gamma_d}{\Gamma_m} = 1$, $T_{e_o} = 0.20T^*$, $\Gamma_{i_o} = -0.01\Gamma_m$**

And the ions' flow

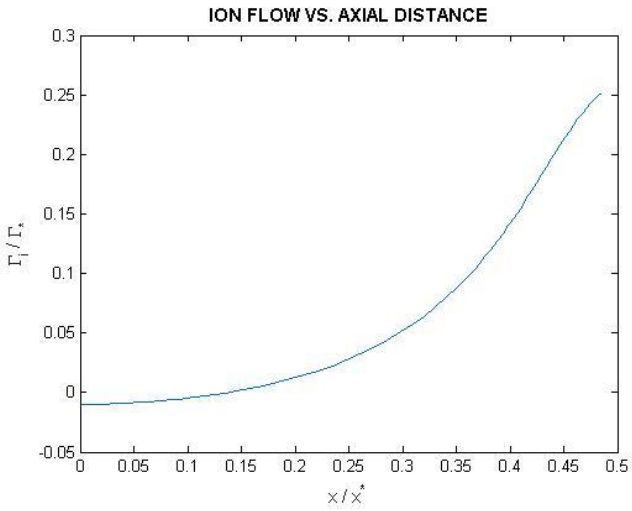

Figure 28. **Variation of ions' flow along a channel with $\frac{\Gamma_d}{\Gamma_m} = 1$, $T_{e_o} = 0.20T^*$, $\Gamma_{i_o} = -0.01\Gamma_m$**

Finally, the most energetic flow for which reasonable physic results are obtained is with an initial temperature of $T_{e_o} = 0.2681T^*$.

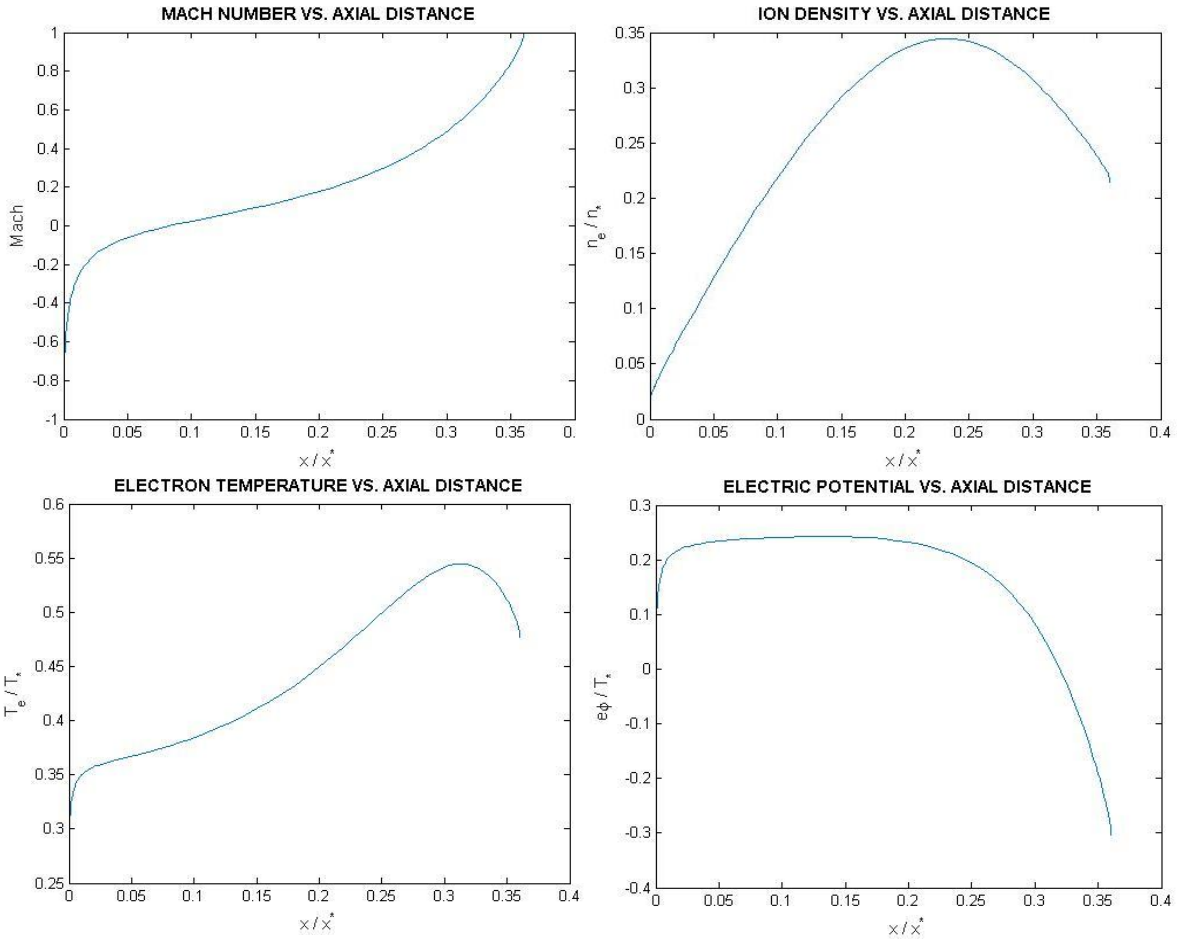

Figure 29. **Plasma variables for a channel with chocked exit, no wall losses and uniform magnetic field with $\frac{\Gamma_d}{\Gamma_m} = 1$, $T_{e_o} = 0.2681T^*$, $\Gamma_{i_o} = -0.01\Gamma_m$**

And the ions' flow

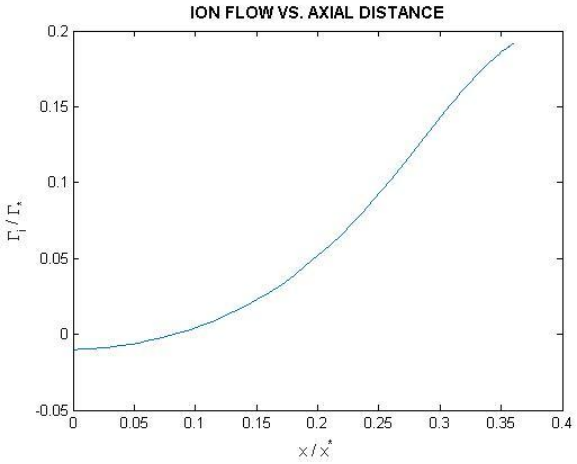

Figure 30. **Variation of ions' flow along a channel with $\frac{\Gamma_d}{\Gamma_m} = 1$, $T_{e_o} = 0.2681T^*$, $\Gamma_{i_o} = -0.01\Gamma_m$**

The most important thing to notice is that the longitude of the channel is shorter with higher initial electron temperatures. This happens because the condition of chocked exit is imposed, so the code integrates the equations until sonic velocity is reached, and the longitude of the channel is an output of the program.

This variation of the initial conditions causes the ionization zone to appear earlier in the channel, so ionization starts earlier. This is logical because the electrons have more energy at the anode and more probabilities of colliding with neutrals. The electrical field grows where ionization happens, so with higher anode electron temperatures, the growth of the electrical field happens earlier, causing the Mach number to increase earlier. As it can be observed comparing figures, the nearly constant Mach zone is reduced and nearly disappears for the limit case. In addition, the fact that the ionization happens earlier also causes this ionization to be more progressive, the growth in the ions' flow is less pronounced, what causes the electrical field to also grow progressively.

In the case of the electrons' density, the peak is reached earlier and it has a lower maximum value of electrons density. In the case of the electrons temperature, the growth is also smoother and the final reached value is decreases with the increase of initial electrons' temperature.

The fact that a channel with a higher initial electrons' energy has lower exit energy means that the process is not being efficient because the energy used to ionize neutrals is low. This is why the ion flow is reduced when increasing T_{e_o}. A chocked Hall thruster with optimum performance would be the one that has null electrons energy at the anode, meaning that all the energy has been used to ionize the inert gas. However, as this is impossible, the goal is to reach the lower possible electron temperatures at the anode.

7. Approximations for different zones

In this chapter every zone inside the Hall thruster is studied in a separate way using the different specific physic mechanisms found.

Following the distribution found in the figure below

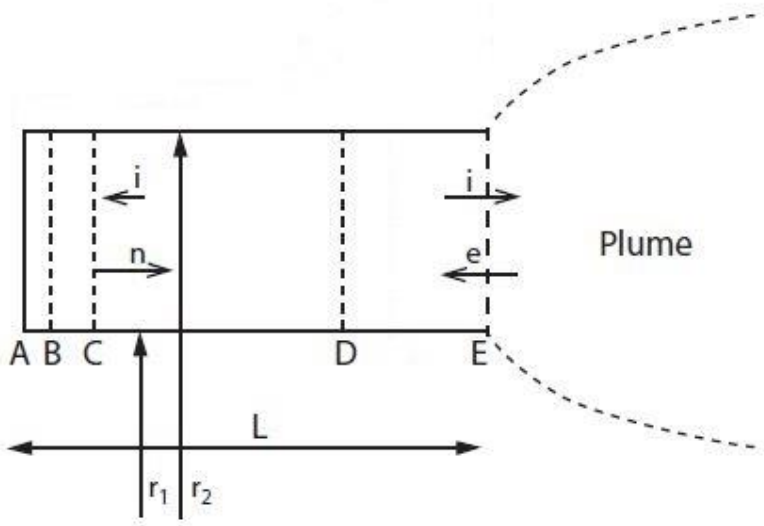

Figure 31. **Zones definition proposed by Martínez-Sánchez (Martínez Sánchez)**

Figure 31 represents the channel of a Hall thruster with an inner radius r_1, an outer radius r_2 and a length L. The small letters n, e and i represent the neutrals, electrons and ions flows respectively. It is important to remember from previous sections that the ions flow is backwards in the first stages (has a reverse sonic point at the anode) and forward in the advanced sections reaching a sonic point at the exit.

Finally the capital letters limit the different zones found in the channel. $A-B$ is the mentioned sheath, a singularity that is considered as a reverse sonic point in our model. Point B denotes the start of quasineutral flow that maintains until the exit. In the quasineutral flow part three different zones can be found: $B-C$ is the presheath zone, $C-D$ is called diffusion zone and $D-E$ ionization region.

In this section a partial analyses for the mentioned regions is offered.

7.1. Presheath and Diffusion Zones

The characteristics of these two zones are closely related, so the treatment that they receive is very similar.

Before arriving to those regions, the electrons have passed the ionization zone, where they lose most of their energy. This fact makes T_e fall to very low levels and causing low levels of ionization in presheath and diffusion zones.

The first approximation is considering that no ionization is made in presheath and diffusion zones, so

$$v_{ion} = 0$$

In order to find a relation between the temperature of the electrons T_e and the velocity of the ions v_i, using the differential equations the following ratio can be written.

$$v_i \frac{\text{equation (79)(79)}}{\text{equation(81)}}$$

Which, remembering that there is no ionization, leaves to

$$\frac{v_i}{k} dv_i = -\frac{5}{2} m_i dT_e$$

Integrating the expression

$$\frac{m_i v_i^2}{2} + \frac{5}{2} kT_e = C_1 \qquad (102)$$

To find the value of the constant it is essential to remember the inverse sonic condition at the inlet

$$v_{i_o} = -\sqrt{\frac{5}{3}\frac{kT_{e_o}}{m_i}}$$

So the value of the constant

$$C_1 = \frac{1}{2}\frac{5}{3} kT_{e_o} + \frac{5}{2} kT_{e_o} = \frac{10}{3} kT_{e_o}$$

Leaving equation **(102)** isolating T_e

$$T_e = \frac{4}{3} T_{e_o} - \frac{m_i v_i^2}{5k} \qquad (103)$$

What can be substituted into equation **(79)** with no ionization.

$$\left(\frac{4}{3}\frac{kT_{e_o}}{v_i^2} - \frac{4}{5} m_i\right) dv_i = m_e v_e \frac{v_e}{v_i} dx = m_e v_e \frac{\Gamma_e}{\Gamma_i} dx$$

Remembering that there is no ionization, the following parameters are considered as constant.

$$\frac{\Gamma_e}{\Gamma_i} = \frac{\Gamma_{e_o}}{\Gamma_{i_o}}$$

$$v_e = v_{e_o}$$

And so the expression above can be integrated, leaving

$$\frac{4}{3}\frac{kT_{e_o}}{v_i} - \frac{4}{5}m_i v_i = C_2 + m_e v_{e_o}\frac{\Gamma_{e_o}}{\Gamma_{i_o}}x \qquad (104)$$

Applying again the reverse sonic condition at the inlet the constant can be found. In this case

$$C_2 = -\frac{8}{5}m_i v_{i_o}$$

So equation **(104)** can be rewritten as

$$\left(\frac{v_i}{v_{i_o}}\right)^2 - 2\left(1 + \frac{5\Gamma_{e_o}m_e v_{e_o}}{8\Gamma_{i_o}m_i|v_{i_o}|}x\right)\left(\frac{v_i}{v_{i_o}}\right) + 1 = 0 \qquad (105)$$

Is at this point where most experts (Dan Goebel, 2008) (Martínez Sánchez) define what they call “presheath thickness” that, as it name shows, is the thickness of the presheath zone.

$$x_{ps} = \frac{8}{5}\frac{\Gamma_{i_o}}{\Gamma_{e_o}}\frac{m_i|v_{i_o}|}{m_e v_{e_o}} \qquad (106)$$

Writing equation **(105)** in terms of the presheath thickness.

$$\left(\frac{v_i}{v_{i_o}}\right)^2 - 2\left(\frac{x}{x_{ps}}\right)\left(\frac{v_i}{v_{i_o}}\right) - 1 = 0 \qquad (107)$$

And isolating $\left(\frac{v_i}{v_{i_o}}\right)$

$$\frac{v_i}{v_{i_o}} = 1 + \frac{x}{x_{ps}} - \sqrt{\left(1 + \frac{x}{x_{ps}}\right)^2 - 1} \qquad (108)$$

The ion velocity expression is found where the negative sign of the square root has been chosen to avoid wrong physical conclusions, as the choice of the positive signed would lead to a flow that decelerates towards sonic.

Substituting equation **(103)** into equation **(81)** this time and following exactly the same process used for obtaining equation **(108)**, the electron temperature expression in the considered zones is found.

$$\frac{T_e}{T_{e_o}} = 1 + \frac{2}{3}\frac{\sqrt{\left(1 + \frac{x}{x_{ps}}\right)^2 - 1}}{1 + \frac{x}{x_{ps}} + \sqrt{\left(1 + \frac{x}{x_{ps}}\right)^2 - 1}} \qquad (109)$$

Since there is no ionization, the density of electrons is easy to evaluate

$$n_e = \frac{\Gamma_{i_o}}{v_i}$$

Substituting the expression found for v_i

$$n_e = \frac{\frac{\Gamma_{i_o}}{v_{i_o}}}{1 + \frac{x}{x_{ps}} - \sqrt{\left(1 + \frac{x}{x_{ps}}\right)^2 - 1}} \quad (110)$$

And, finally, the electric field is obtained from equation **(70)**, that can be integrated considering that there is no ionization. Using the initial reverse sonic condition to find the integration constant as usual, the expression below is obtained.

$$\frac{m_i v_i^2}{2} + e\phi = \frac{m_i v_{i_o}^2}{2}$$

The procedure used to obtain the final expression is the same used before so it is not included. The final expression for the electric field in the presheath and diffusion zone is

$$\phi = \frac{5}{3}\frac{kT_{e_o}}{e} \frac{\sqrt{\left(1 + \frac{x}{x_{ps}}\right)^2 - 1}}{1 + \frac{x}{x_{ps}} + \sqrt{\left(1 + \frac{x}{x_{ps}}\right)^2 - 1}} \quad (111)$$

7.1.1. Simplified expressions for Diffusion zone

The expressions found before are valid for zones with quasineutral plasma and no ionization, in other words, for both the presheath zone and the diffusion zone.

However, it is known by previous studies (Dan Goebel, 2008) that the presheath zone is considerably thinner than the diffusion zone.

Studying the equations for $x \gg x_{ps}$, what is obtained are the expressions or the limits of the different values in the diffusion zone. So, the condition to study is

$$\frac{x}{x_{ps}} \to \infty \quad (112)$$

The limits of the different expressions for this condition can be found.

In the case of the ions' velocity v_i

$$\lim_{\frac{x}{x_{ps}} \to \infty} \left(1 + \frac{x}{x_{ps}} - \sqrt{\left(1 + \frac{x}{x_{ps}}\right)^2 - 1}\right) = \infty - \infty$$

Solving the mathematical indetermination

$$\lim_{\frac{x}{x_{ps}}\to\infty}\left(1+\frac{x}{x_{ps}}-\sqrt{\left(1+\frac{x}{x_{ps}}\right)^2-1}\right)=-\frac{x_{ps}}{2x}$$

So the ions' velocity tends to

$$v_{i_{diffusion}}\to v_{i_o}\frac{x_{ps}}{2x} \tag{113}$$

Doing the same for the electrons temperature

$$\lim_{\frac{x}{x_{ps}}\to\infty}\left(1+\frac{2}{3}\frac{\sqrt{\left(1+\frac{x}{x_{ps}}\right)^2-1}}{1+\frac{x}{x_{ps}}+\sqrt{\left(1+\frac{x}{x_{ps}}\right)^2-1}}\right)=1+\frac{2}{3}\frac{\infty}{2\infty}=1+\frac{2}{6}=\frac{4}{3}$$

In this case it is found that the electrons' temperature is asymptotic.

$$T_{e_{diffusion}}\to\frac{4}{3}T_{e_o} \tag{114}$$

Following with the study of the study of the density of electrons

$$\lim_{\frac{x}{x_{ps}}\to\infty}\left(\frac{1}{1+\frac{x}{x_{ps}}-\sqrt{\left(1+\frac{x}{x_{ps}}\right)^2-1}}\right)=\frac{1}{\infty-\infty}$$

Solving the mathematical indetermination

$$\lim_{\frac{x}{x_{ps}}\to\infty}\left(\frac{1}{1+\frac{x}{x_{ps}}-\sqrt{\left(1+\frac{x}{x_{ps}}\right)^2-1}}\right)=\frac{2x}{x_{ps}}$$

Then the density of electrons tends to

$$n_{e_{diffusion}}=\frac{\Gamma_{i_o}}{v_{i_o}}\frac{2x}{x_{ps}} \tag{115}$$

Finally, studying the behavior of the electrical field

$$\lim_{\frac{x}{x_{ps}}\to\infty}\left(\frac{5}{3}\frac{kT_{e_o}}{e}\frac{\sqrt{\left(1+\frac{x}{x_{ps}}\right)^2-1}}{1+\frac{x}{x_{ps}}+\sqrt{\left(1+\frac{x}{x_{ps}}\right)^2-1}}\right)=\frac{5}{3}\frac{kT_{e_o}}{e}\frac{\infty}{2\infty}=\frac{5}{6}\frac{kT_{e_o}}{e}$$

So, the electrical field is also asymptotic and tends to

$$\phi\to\frac{5}{6}\frac{kT_{e_o}}{e} \qquad (116)$$

7.1.2. Plotted functions

Plotting the functions **(108)**, **(109)**, **(110)**, **(111)** obtained in the section above.

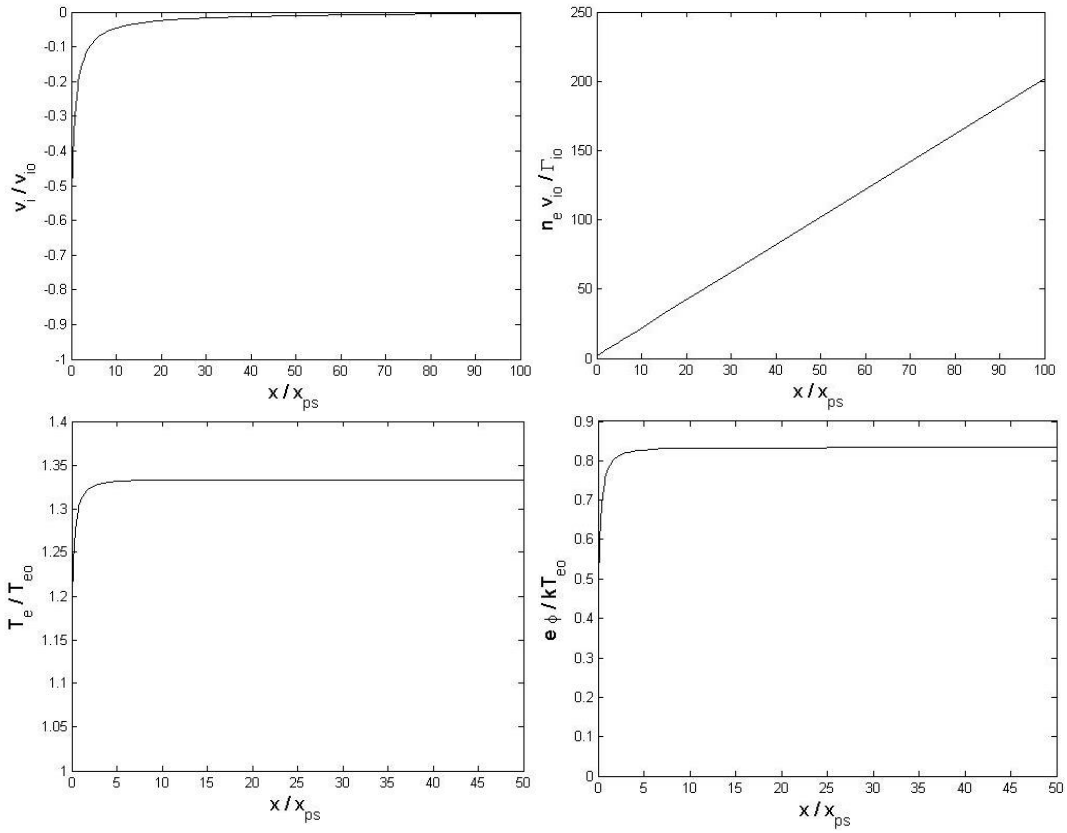

Figure 32. **Presheath and diffusion zone distribution of variables**

The tendencies predicted by the equations are perfectly satisfied with these plots. Let's analyze each variable individually.

In the case of the ions velocity, the reverse sonic point at the anode condition is met and tends to a very small negative value while advancing through the channel in the diffusion zone as predicted by **(113)**. That behavior is very similar to the presented by other one-dimensional models as well as in keeping with

results obtained by the numerical model. It also shows that the great acceleration of the ions is fully carried out in the ionization zone.

Talking about the electrons' density, it tends to a perfect straight line even in the early positions in the channel. This fact agrees with condition **(115)** and is also very similar to the observed in **Figure 23**, where, in the initial zone of the channel, the density of electrons grows in a linear way. In addition, it is possible to affirm that the peak and drop of this density happens in the ionization zone.

The same happens for the electrons' temperature. During the diffusion zone, where the electrons have lost most of their energy, the temperature is approximately constant in a low value as showed by **Figure 23** and expected by condition **(114)**. It is obvious that the drop in temperature happens in the ionization zone because the energy is dissipated precisely by the ionization.

Finally, the electrical field has the expected behavior by equation **(116)** because it tends to a low value in both the presheath and diffusion zones. The growth observed in **Figure 23** happens entirely on the ionization zone, where the number of ions increases significantly and so, with the growth of the electrical field, the acceleration is higher.

7.2. Ionization zone

From the results of the differential equations in **Figure 23** it seems obvious that after the diffusion zone, there is a different zone where the parameters change drastically. This zone is called ionization zone.

The main characteristic of this zone is that the electrons are more energetic (T_e is higher) and so, ionization occurs. Consequently, the density of electrons is reduced and a forward electrical field E_x appears.

However, studying the variation of both the electrons temperature T_e and the electrical field ϕ is too complicated and would suppose a whole new level of approximation that escapes from the limits of the project. Even so, what a simple analysis is capable of is studying the study of the transition zone to the ionization zone where the electrons temperature T_e is already notably higher than in the diffusion zone, but ϕ is still negligible.

The aim of this approximation is finding an expression that, given physical inputs, finds the initial value T_{e_o} that permits calculating the sonic velocity at the anode v_{i_o}.

To obtain it, the electron energy equation **(74)** is used and the integration constant evaluated at the diffusion zone where, remembering condition **(114)**, $T_{e\,diffusion} \to \frac{4}{3} T_{e_o}$ and that $E_x \sim 0$. It is obtained

$$\Gamma_e\left(\frac{5}{2}kT_e + E_i'\right) = \Gamma_{e_o}\left(\frac{10}{3}kT_{e_o} + E_i'\right) \quad (117)$$

Using also the electron momentum equation **(70)** with the same approximations.

$$n_e kT_e = -m_e \Gamma_e \nu_e x \quad (118)$$

It is known from other analysis (Ahedo & Martínez-Sánchez) (Dan Goebel, 2008) that in the diffusion zone the following condition is accomplished

$$kT_e \sim \frac{3}{4}E_i \quad (119)$$

The three conditions **(117)**, **(118)**, **(119)** and getting them together it is obtained

$$xdx = \frac{k^2 T_e dT_e}{m_e \upsilon_e \upsilon_{ion}\left(kT_e + \frac{2}{5}E_i'\right)} \quad (120)$$

The last step is integrating expression **(120)**. But it is not trivial, because υ_{ion} has a dependence on T_e that affects the exponential $e^{-\frac{E_i}{kT_e}}$, which is especially strong in the zone considered because $kT_e \ll E_i$.

Some approximation is necessary in the term

$$\frac{k^2 T_e dT_e}{\upsilon_{ion}}$$

Substituting $\upsilon_{ion} = ce^{-\frac{E_i}{kT_e}}$, where c is the mean velocity of the electrons as usual,

$$\frac{k^2}{c}T_e e^{\frac{E_i}{kT_e}}dT_e \cong -\frac{(kT_e)^3}{E_i}d\left(\frac{1}{\upsilon_{ion}}\right)$$

Ignoring weaker terms it can finally be approximated

$$\frac{k^2 T_e dT_e}{\upsilon_{ion}} = -\frac{1}{E_i}d\left[\frac{(kT_e)^3}{\upsilon_{ion}}\right] \quad (121)$$

Rewriting equation **(120)** with the approximation **(121)**

$$xdx = \frac{1}{m_e \upsilon_e E_i\left(kT_e + \frac{2}{5}E_i'\right)}d\left[\frac{(kT_e)^3}{\upsilon_{ion}}\right] \quad (122)$$

Expression that, if evaluated in the diffusion part, where $T_e = \frac{4}{3}T_{e_o}$, can be easily integrated obtaining

$$L^2 = \frac{\frac{128}{27}\left(kT_{e_o}\right)^3}{m_e \upsilon_e \upsilon_{ion} E_i\left(\frac{4}{3}kT_{e_o} + \frac{2}{5}E_i'\right)} \quad (123)$$

The expression found perfectly accomplishes the goals set at the beginning of the transition to the ionization zone study; given input parameters such as the

length of the channel or the magnetic field, it permits finding the electrons temperature at the anode T_{e_o} and, consequently, the sonic velocity at the reverse sonic point v_{i_o}.

8. Thrust

Unfortunately, despite the tendencies and exit values showed by the model are correct, the fact that one-dimensional, no plume and no loses simplifications have been adopted, calculating the thrust given by the thruster using numerical methods would not give reliable results.

However, for the sake of completeness, an analytical study of the thrust has been included.

8.1. Unidirectional, singly ionized monoenergetic Hall thruster

The trust can be defined in a thruster as the change of momentum in time.

$$T = \frac{d}{dt}\left(m_p v_x\right) \tag{124}$$

In a gross approximation, equation **(124)** can be written as the product of the propellant mass flow and the velocity at the exit.

$$T = \dot{m}_p v_x \tag{125}$$

However, when considering the propellant, two types of particles come into mind; the neutrals and the ions. In almost every analysis the neutrals can be neglected as their velocity is more than a hundred times lower than the ions' velocity. So equation **(125)** is now

$$T = \dot{m}_i v_i$$

Where the ion velocity is given by the previous equation **(22)**, to refresh memory

$$v_i = \sqrt{\frac{2eV_b}{M}}$$

Where e is the electron charge, V_b the voltage through which the ion is accelerated and M is the ion's mass.

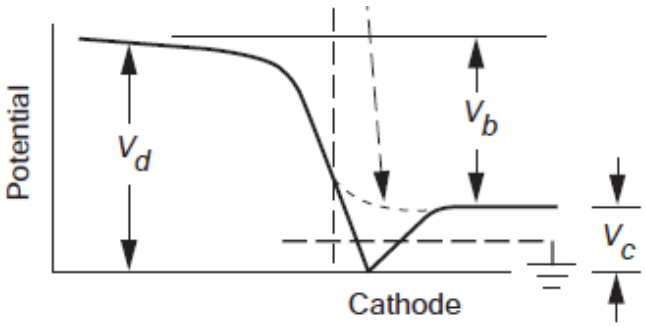

Figure 33. **Definition of beam current (Dan Goebel, 2008)**

Before going on, it is important to notice that the beam voltage V_b is not exactly the voltage at the array V_a. The beam voltage accounts for a diminution on the potential outside the channel, at the plume, due to the presence of the cathode. This diminution is V_c and has typical values between 10 and 20 Volts. So

$$V_b = V_a - V_c = V_a - 15$$

Continuing with the analysis of the thrust

$$T = \dot{m}_i \sqrt{\frac{2eV_b}{M}}$$

Where the ions mass flow can be substituted by the equivalent equation

$$\dot{m}_i = \frac{I_b M}{e}$$

Where I_b is the ion's beam current. Finally the thrust reads as follows.

$$T = I_b \sqrt{\frac{2MV_b}{e}} \qquad (126)$$

The equation above is only true for a singly ionized, unidirectional and monoenergetic beam of ions. Some corrections can be applied.

8.2. Corrected expression

Two corrections are proposed in theoretical studies (Dan Goebel, 2008): correction for the divergence (two-dimensional effects) of the beam and for the presence of doubly ionized atoms.

Starting with the correction for the divergence of the beam; in the case studied, a thruster with assumed constant ion current density profile, it is only necessary to account for the contribution of the velocity parallel to the axis of the thruster. So the correction factor is

$$\beta = cos\theta$$

Where θ is the average half-divergence angle of the beam.

On the other hand, when analyzing the effects of double ionized atoms, the first important feature is that the total ions' current is the sum of single and double ionized atoms' currents.

$$I_b = I^+ + I^{++} \qquad (127)$$

Where I^+ is the current of single ionized atoms current and I^{++} double ionized.

So the thrust is the sum of both contributions

$$T = T^+ + T^{++} = N^+ v^+ AMv^+ + N^{++} v^{++} AMv^{++}$$

Introducing the variable e

$$T = (N^{+}v^{+}Ae)\frac{M}{e}v^{+} + (N^{++}v^{++}A2e)\frac{M}{2e}v^{++}$$

Substituting the value of velocities and introducing the intensities

$$T = (I^{+})\frac{M}{e}\sqrt{\frac{2V_b e}{M}} + (I^{++})\frac{M}{2e}\sqrt{\frac{4V_b e}{M}}$$

Rewriting the whole expression

$$T = \sqrt{\frac{2V_b M}{e}}\left(I^{+} + \frac{1}{\sqrt{2}}I^{++}\right) \quad (128)$$

From comparison between equations **(126)** and **(128)**, it can be extracted that the corrective factor is

$$\alpha = \frac{I^{+} + \frac{1}{\sqrt{2}}I^{++}}{I_b} = \frac{I^{+} + \frac{1}{\sqrt{2}}I^{++}}{I^{+} + I^{++}} \quad (129)$$

As can be deduced, α is minor than 1, so the effect of double ionized atoms is negative for the thrust. The extra energy used for the second ionization affects to the velocity with a factor $\frac{1}{\sqrt{2}}$.

Finally the total correction factor is the product of the two found.

$$\gamma = \alpha\beta \quad (130)$$

Where γ has typical values of $\gamma = 0.958$ with a 10% of double ionization rate.

The corrected thrust is

$$T = \gamma I_b\sqrt{\frac{2MV_b}{e}} \quad (131)$$

8.3. Expression validation

To ensure the corrections are properly deduced, the thrust obtained for typical combinations of values of I_b and V_b has been plotted.

The figure obtained is

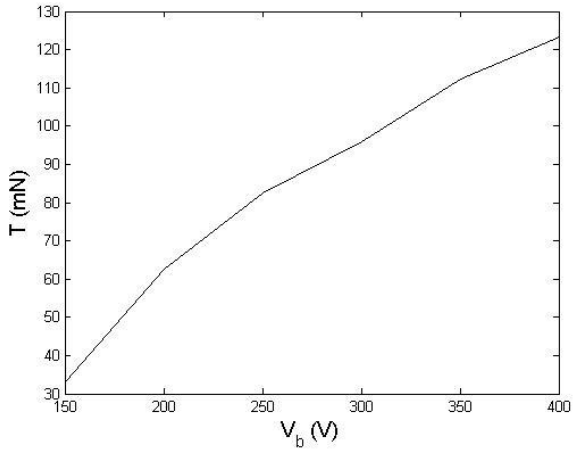

Figure 34. **Thrust behavior in front of different beam voltages**

As expected, the thrust grows when the beam voltage increases. This plot is in accordance with other articles that tested both experimentally and analytically the thrust (Garrigues, Boyd, & Boeuf, 2001). An example can be seen below.

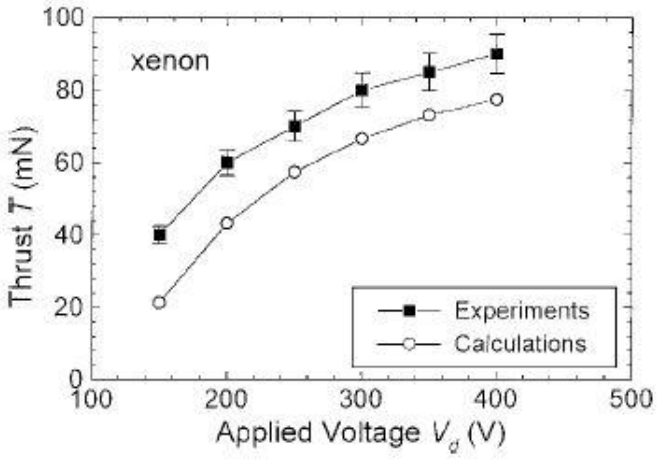

Figure 35. **Thrust behavior in front of different beam voltages (Garrigues, Boyd, & Boeuf, 2001)**

The tendency obtained of the thrust growing when the beam voltage increases is confirmed.

However, it is essential to remember conclusions obtained in the previous analytical study: despite the thrust grows with the input voltage, the efficiency reaches a maximum and starts falling, so greater applied voltages do not mean better performance, the key is working on the point where efficiency is at its maximum.

9. Conclusions and Future Work

In the first part of the project, analysis of low-thrust transfer orbits from LEO to GEO and comparisons with conventional transfers have been dealt with.

From the computation of parameters in low-thrust orbits it is extracted that the constant acceleration given to the spacecraft, and thus the thrust, have an enormous influence on the transfer time. By multiplying this acceleration per ten, the transfer time is also divided per ten.

Another surprising feature found is that using different constant thrusts to perform a low-thrust transfer does not affect the amount of fuel needed. The fact that a higher thrust needs higher fuel consumption is balanced with the reduction of transfer time produces by the higher thrust. All in all, the amount of fuel needed only depends on the distance between initial and final orbits.

By combining the two previous characteristics, it is logical to think that the perfect regime for a transfer using Hall Thrusters is with maximum thrust, because the transfer time will be the minimum possible without affecting fuel consumption.

The comparison between low-thrust and Hohmann transfers showed that when increasing the altitude of the initial orbit, the low-thrust transfer time was reduced (nearly 10 days less if starting from 2000 km instead of 200 km), but in the case of the Hohmann transfer the time slightly increased although in a completely different scale (about 20 minutes difference between starting from 2000 km instead of 200 km). However the total time needed to perform the transfer is much greater when using a Hall thruster instead of conventional propulsion (of the order of 50 days in front of 5 hours).

The strength of Hall thruster came when computing the fuel needed to perform the transfer. In a low-thrust transfer the amount of fuel needed is nearly ten times lower than in a Hohmann transfer. This is possible thanks to the incredible specific impulse given by Hall thrusters that, despite needing a larger Δv in a low-thrust transfer than in a Hohmann transfer, reduces the fuel consumption, which is translated into saving money. Besides, the quantity of fuel saved increases with the distance between initial and final orbits; because of this Hall thrusters are very popular in deep-space missions.

It is estimated that the amount of money saved in a LEO to GEO transfer, just for the simple fact of needing to launch less weight due to propellant reduce, is of about 10 million dollars.

All in all, from the first half of the project, it is extracted that Hall thrusters are a great solution for private companies or public institutions that need to launch a satellite (e.g. communication satellites) and want to reduce costs. On the other

hand, time is an important restriction; Hall thrusters cannot be used in urgent missions where the time needed to perform them must be short. Companies must evaluate if having the satellite in orbit a month later is worth it 10 million dollars.

Therefore it refers to the second part of the project, the analytical analysis was contrasted with experimental data and confirmed the behaviors predicted. Increasing the voltage of the array increases the thrust and the efficiency. However, the efficiency reaches a limit when the ionized fraction of the gas is already very high and cannot grow more and starts to fall. This is precisely the point where Hall thrusters need to work; the perfect combination of high thrust with the maximum efficiency possible produced by high ionization.

Later, the one-dimensional model developed showed to be a good approximation for the study of variables inside the Hall thruster as well as obtained exit values adequate to the simplifications adopted. However, presented the typical discrepancies caused by neglecting the plume, two-dimensional and wall loses effects.

The distribution of Mach number satisfies the initial reverse sonic condition and the chocked exit condition. The velocity of the ions slowly grows, turning positive before ending the diffusion zone, and suffers a great acceleration at the ionization zone where the electrical field is stronger. The exit velocity is Mach one because it is a chocked exit.

The numerical results for the electrons' density coincide with other numerical analysis; the density grows nearly linearly, reaches a maximum and starts decaying when the electrons are more energetic in order to maintain plasma neutrality. At the ionization zone it falls to a low value, the density of electrons at the exit.

The electrons temperature has also the adequate behavior; high at the energetic zones and low at the diffusion zone. The exit value is reasonable and permits calculating the exit velocity with all the precision permitted by the approximations adopted.

Studying the plot of the distribution along the channel of ϕ, it can be realized that not only it is similar to other results, but also is in perfect accordance with the distribution of velocity. When ionization happens, ϕ decreases rapidly, so, remembering that $E_x = -\frac{d\phi}{dx}$, the electrical field grows to a high positive value accelerating the ions created to the exit of the channel where they reach sonic velocities.

Both the approximations for the diffusion zone of T_e and ϕ are in accordance with the differential equations resolution results.

The variation of the initial conditions showed that having greater electrons energies at the anode is detrimental for the efficiency of the process, as the energy used to ionize neutrals is lower. Despite lower ionization efficiencies make the curves to be smoother, the lowest energy possible for the electrons at the anode has to be sought in order to increase performance capabilities

Finally, the study of the thrust confirmed that it grows when the applied voltage is greater, but that does not mean better performance as the efficiency reaches a maximum and falls; the point with better efficiency must be sought.

For the future, several extensions can be made, starting with the introduction of a variable magnetic field along the channel, with a higher value at the ionization zone in order to improve the thruster's properties. Also a consideration of the plume can be added; the presence of the plume modifies the final values at the channel in order to maintain continuity and performs an extra contribution to the thrust.

To increase even more the strength of the code, two-dimensional effects can be included both in the channel and the plume and walls loses by recombination of ions and electrons considered. A proposed method for implementing bi-dimensional effects is the "Particle in cell" method applied to Hall thrusters. This method has been studied recently by Prof. Ahedo and has some very interesting features. It is a method that solves partial differential equations systems where particles are tracked in a continuous phase space and properties such density and current are computed on mesh points.

If disposing of the adequate resources, experimental analysis of real Hall thrusters can be helpful to detect weak points of the code and polish it to perfection.

Bibliography

Ahedo, E., & Martínez-Sánchez, M. (s.f.). One-Dimensional Plasma Structure in Hall Thrusters.

Boever, Kiim, Koroteev, Latyshev, Morozov, Popov, et al. (1991). *State of the Works of Electrical Thrusters in the USSR.* Viareggio, Italia: 22nd International Propulsion Conference.

Brophy, J. R. (2002). NASA's Deep Space 1 Ion Engine. *Review Scientific Instruments, 73*, 1071-1078.

Case Western Reserve University. (2013). *Hohmann Transfer Orbits*. Retrieved March 16, 2016, from http://burro.astr.cwru.edu/Academics/Astr221/Gravity/transfer.html

Dan Goebel, I. K. (2008). *Fundamentals of Electric Propulsion: Ion and Hall Thrusters.* California, USA: NASA.

European Space Agency. (3 de April de 2013). *Telecommunications & integrated applications*. Retrieved March 16, 2016, from http://www.esa.int/Our_Activities/Telecommunications_Integrated_Applications/Orbits

Fitzpatrick, R. (s.f.). *Introduction to plasma physiscs.* The University of Texas at Austin, Physics Department. Austin: The University of Texas at Austin.

G. Seikel, E. R. (1962). *Hall Current Ion Accelerator* (Vol. 7). Am. eries 11.

Garrigues, L., Boyd, I., & Boeuf, J. (July de 2001). Computation of Hall Thruster Performance. *Journal of Propulsion and Power, XVII*(4).

Gedalin, M. (s.f.). Introduction to Plasma Physics. En M. Gedalin, *Lecture Notes in Physics.*

Goddart, R. (1906). *The Green Notebooks* (Vol. 1). Worchester, Massachusetts, USA: Clark University.

Haas, J. M., Gulczinski III, F. S., & Gallimore, A. D. (s.f.). Performance Characteristics of a 5 kW Laboratory Hall Thruster.

Herrera, E., & Masdemont, J. (n.d.). *Study of LEO to GEO transfers via the L1 Sun-Earth or Earth-Moon libration points.* Universitat Politècnica de Catalunya, Mathematics Department. Barcelona: Universitat Politècnica de Catalunya.

Iowa State University. (2001). *Polaris Project Evening Star*. Retrieved March 15, 2016, from, de http://www.polaris.iastate.edu/EveningStar/Unit4/unit4_sub3.htm

Jacob Blaustein Intitutes for Desert Research. (n.d.). *Remote Sensing Laboratory Venus Mission*. (B.-G. U. Negev, Editor) Retrieved April 14, 2016, from Remote Sensing Laboratory: http://www.bgu.ac.il/BIDR/research/phys/remote/VENuS/VENuS-TechMission.htm

Komurasaki, K., Hirakowa, M., & Arakawa, Y. (1991). IEPC. *22nd Electric Propulsion Conference*, (págs. 91-178). Viareggio.

Koppel, C. R., & Estublier, D. (2005). *The SMART-1 Hall Effect Thruster around the Moon: In Flight Experience.* Princeton, New Jersey, USA: 29th International Electric Propulsion Conference.

Krulle, & Zeyfang. (1975). *Preliminary Conclusions of Applied Field Electromagnetic Thruster Research at DFVLR.* New Orleans, USA: Electric Propulsion Conference.

Martínez Sánchez, M. (s.f.). *Hall Thrusters Lecture.* Boston, Massachusetts, USA: Massachusetts Institute of Technology.

Mel'kumov, T. M. (1911). *Pioneers of Rocket Technology. Selected Works.* (NASA, Trad.) Moscow, Russia: Institute for the History of Natural Science and Technology.

NASA. (2006, August 23). *Glench Research Center at Lewis Field*. Retrieved March 15, 2016, from http://www.grc.nasa.gov/WWW/hall/future/future.htm

Pidgeon, D. J., Corey, R. L., Sauer, B., & Day, M. L. (2006). *Two Years On-Orbit Performance of SPT-100 Electric Propulsion.* San Diego, California, USA: 24th AIAA INternational Communications Satellite Systems Conference.

Pote, B., & Tedrake, R. (n.d.). Performance of a High Specific Impulse Hall Thruster.

Stansbury, S. (2009, December 10). *Low Thrust Transfer to GEO: Comparison of Electric and Chemical Propulsion.* (C. C. Research, Ed.) Retrieved March 26, 2016, from http://ccar.colorado.edu/asen5050/projects/projects_2009/stansbury/

Widnall, S., & Peraire, J. (2008). *Orbit Transfers and Interplanetary Trajectories.* MIT, Dynamics Deprtment. Boston: MIT.

Wikipedia. (10 de March de 2016). *Low Earth Orbit*. Retrieved March 15, 2016, from https://en.wikipedia.org/wiki/Low_Earth_orbit

Wilson, J. (2016, January). *Hohmann Transfers*. Retrieved March 16, 2016, from http://jwilson.coe.uga.edu/EMAT6680Fa05/Bacon/hohmanntransfers.html

Yushmanov, Y. (1958). *Radial Potential Distribution in the Cylindrical Trap with the Magnetron Method of Injecting the Ions* (Vol. 4). USSR: Phys. of Plasma of Controlled Thermonuclear Fusion.